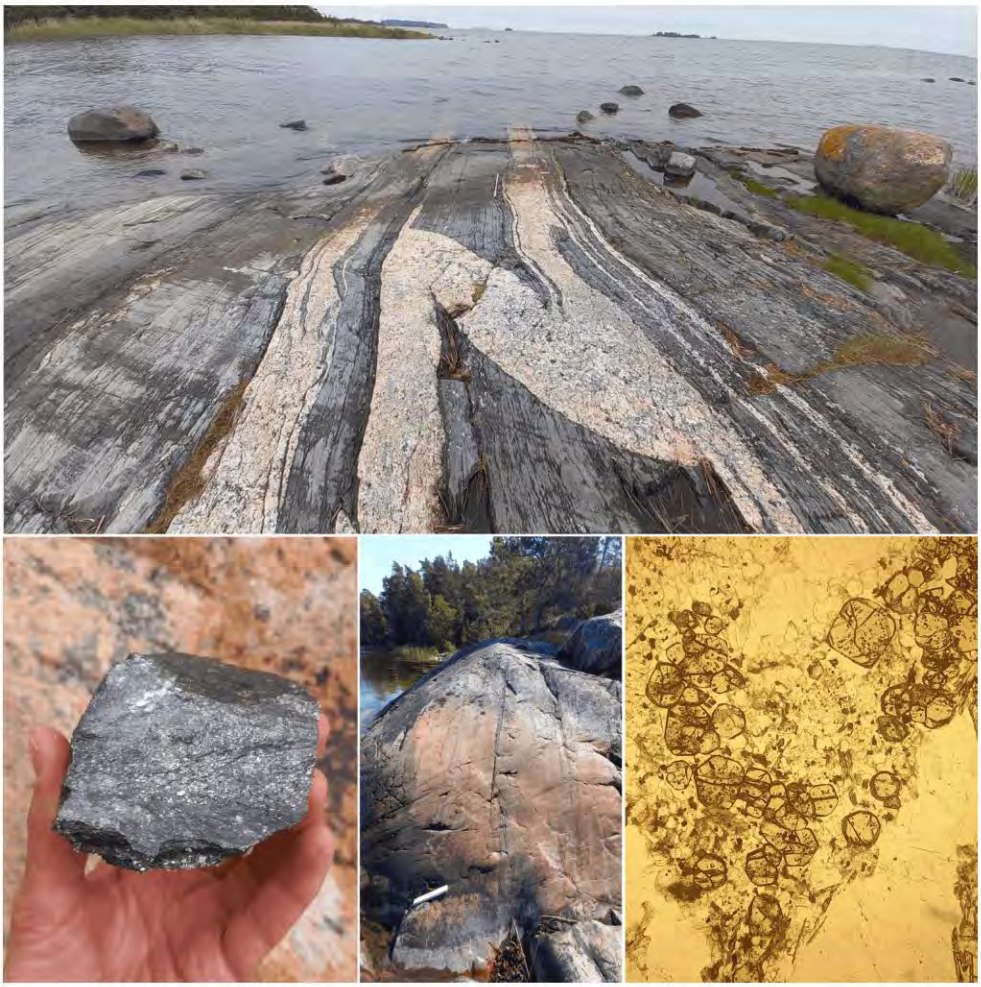
Stockholm University

Bachelor Thesis

Degree Project in
Geological Sciences, 15 hp

The supracrustal succession on Östra Lagnö, Stockholm archipelago

Jasmin Gelinck



Stockholm 2026

Department of Geological Sciences
Stockholm University
SE-106 91 Stockholm

Contents

1 ABSTRACT 4
2 INTRODUCTION 4
2.1 Terminology 4
2.2 Regional geological history: Bergslagen & Utö 4
3 METHODS 5
3.1 Fieldwork 5
3.2 Geological mapping 5
3.3 Petrographic analysis 5
3.4 SEM analysis 6
4 RESULTS 6
4.1 Felsic volcanic rocks 11
4.2 Mafic rocks 14
4.3 Possible sedimentary and volcaniclastic units 14
4.4 Intrusive felsic rocks 17
4.5 Structural observations 19
4.6 Site 28 / Rävnäsudden 21
4.7 Mineralogical observations 22
4.7.1 Garnet 22
4.7.2 Amphiboles 25
4.8 Other minerals 26
5 DISCUSSION 28
5.1 Geological succession and depositional history 28
5.1.1 Regional depositional context 28
5.2 Minerals and metamorphism 29
5.2.1 Metamorphic grade 30
5.3 Regional metamorphic context 31
5.4 Structural evolution and deformation 31
5.5 Intrusive history and relative chronology 33
6 CONCLUSION: THE GEOLOGICAL EVOLUTION OF ÖSTRA LAGNÖ 33
6.1 Limitations and further research 34
7 REFERENCES 35
8 APPENDIX 36

Acknowledgements

I want to thank my supervisor, Joakim Mansfeld, for answering all my questions and remaining patient and kind throughout the entire process.

I also want to thank Alasdair Skelton, and the Geological Department, for the possibility of doing a distance degree, and funding this study.

1 ABSTRACT

This study investigates the supracrustal succession on the island of Östra Lagnö (easternmost part of Ljusterö) in the Stockholm archipelago. The aim was to reconstruct the metamorphic history of Östra Lagnö and compare it regionally to draw parallels and identify differences. This was done utilising geological field mapping and petrographic examination, including SEM-EDS. The results reveal a succession dominated by felsic metavolcanic and metavolcaniclastic rocks with subordinate sedimentary intercalations, mafic units, and polyphase granitoid intrusions. Sedimentary features suggest deposition in a subaqueous environment. Mineral assemblages including pargasitic amphibole, garnet, plagioclase, and biotite indicate amphibolite facies metamorphism. The presence of abundant Fe- and Mg-rich minerals such as garnet and amphibole in felsic host rocks locally records pre-metamorphic hydrothermal alteration. Metamorphic mineral growth, deformation, and intrusive activity overlapped rather than occurring as separate events. The succession is consistent with Palaeoproterozoic volcanic-sedimentary sequences described elsewhere in Bergslagen.

2 INTRODUCTION

Östra Lagnö, situated in the northern Stockholm archipelago, Sweden, forms part of the Bergslagen region of the Svecofennian province and comprises Palaeoproterozoic supracrustal and intrusive rocks that were subsequently affected by metamorphism and deformation during the Svecokarelian orogeny. Although the geology of Bergslagen has been extensively investigated (Allen et al., 1996; Stephens and Jansson, 2020), comparatively little detailed research has focused specifically on Östra Lagnö. Its geology has instead primarily been documented as part of broader investigations of the Ljusterö area, with Lundqvist's 1962 paper "Det svekofenniska suprakrustalstråket mellan Ljusterö och Rödlöga i Stockholms norra skärgård" (translated throughout this study from Swedish) providing one of the principal detailed descriptions. This study therefore aims to contribute to understanding the geological history and regional relationships of the supracrustal rocks of eastern Bergslagen.

The study aims to characterise the lithology, structural relationships, and metamorphic evolution of the supracrustal rocks of Östra Lagnö and to reconstruct their geological history through field mapping, analysis of field relationships, petrographic investigation, and mineral-chemical analysis. Particular attention is given to the identification and interpretation of the original protoliths, intrusive relationships, and the effects of subsequent metamorphism and deformation.

The results are used to revisit previous interpretations of the area, place Östra Lagnö within the broader geological framework of Bergslagen, and assess similarities and differences with the better-studied supracrustal succession on Utö. A further objective is to produce a geological map of Östra Lagnö, integrating field observations with petrographic interpretations.

2.1 Terminology

All lithological units in the study area have been metamorphosed; for brevity, the prefix *meta-* is therefore omitted where this is clear from context. Metamorphic recrystallisation has, to varying degrees, affected primary textures throughout the succession; where this relates to a specific observation it is noted in context. Pyroclastic terminology such as "lapilli" and "fiamme" is likewise used descriptively, on the basis of size, shape and texture, without asserting a confirmed pyroclastic origin unless stated; a qualifier (e.g. "possible") is used instead where that origin is itself in doubt.

2.2 Regional geological history: Bergslagen & Utö

Östra Lagnö, in the Ljusterö area of the Stockholm archipelago, lies in the southeastern part of the Bergslagen region. Bergslagen is located in the Svecofennian province of the Fennoscandian Shield, which forms the exposed Precambrian core of the East European Craton. During the Palaeoproterozoic, subduction-related magmatism generated extensive volcanic activity, while extensional intra-arc and/or back-arc environments have been proposed for the development of volcanic centres and associated basins (Allen et al., 1996).

At approximately 1.91-1.89 Ga, predominantly felsic volcanic activity produced extensive calc-alkaline volcanic and volcaniclastic successions. Explosive volcanism generated abundant pyroclastic material, while reworking of volcanic material and periods of reduced volcanic activity permitted siliciclastic and carbonate sedimentation

within the succession (Allen et al., 1996). Calc-alkaline granitoids were emplaced during continued magmatic activity (Stephens and Jansson, 2020).

The subsequent convergence and crustal shortening during the Svecokarelian orogeny affected the volcanic, sedimentary and intrusive rocks by polyphase deformation and regional metamorphism. Metamorphic grade varies across Bergslagen, predominantly from greenschist to amphibolite facies, with locally higher-grade conditions, but primary volcanic and sedimentary features may nevertheless remain preserved (Andersson et al., 2006; Skelton et al., 2018). Later anatectic and intrusive magmatism further modified parts of the region (Stephens and Jansson, 2020).

The rocks investigated on Östra Lagnö form part of this complex Palaeoproterozoic geological framework and can therefore be compared with both the wider Bergslagen succession and the supracrustal succession on nearby Utö.

3 METHODS

3.1 Fieldwork

Fieldwork was conducted from 11 to 18 June 2026 on Östra Lagnö and the easternmost part of Västra Lagnö. Observation sites were selected according to the availability and accessibility of bedrock exposures, with fieldwork concentrated along the coastline where exposure was maximal.

A total of 40 main sites and 19 associated sub-sites were examined (Figure 1). At each site, lithology, mineralogy, textures, foliation, deformation, and geological contacts were recorded, with particular attention to primary or relict features and mineral relationships. Outcrops were documented photographically, and coordinates were recorded using Google Maps. Scale objects in field photographs include a hand lens (~3cm), folding ruler (~22cm folded), and compass (~10cm).

Structural measurements were taken where suitable features were identified. Strike and dip measurements were primarily obtained from lithological layering and foliation, while the orientation of elongated clasts was recorded at selected localities.

A total of 18 rock samples were collected from representative lithologies and features, of which 11 were prepared for petrographic analysis at Stockholm University. Site numbers refer to field localities, whereas sample numbers identify collected specimens and do not necessarily correspond to the associated Site numbers.

No dilute HCl was available during fieldwork, limiting field identification of carbonate minerals. Therefore, carbonate rocks were identified primarily from weathering characteristics, mineral makeup, and field appearance.

3.2 Geological mapping

A geological map of the study area was produced in QGIS using Lantmäteriet Topografi 10 Nedladdning vektor topographic data as the base. The map was constructed in the SWEREF 99 TM (EPSG:3006) coordinate reference system. Geological symbols used on the map are a combination of standard QGIS symbols, author-created symbols, and symbols adapted from the GISsymbology symbol collection, licensed under CC BY-SA 4.0.

The lithological boundaries were based on exposed contacts. As field observations were largely restricted to coastal bedrock exposures, their mapped polygons were extended a short distance inland to illustrate interpreted lithological continuity. Mapping confidence was limited where bedrock was obscured by vegetation, buildings, or other development.

3.3 Petrographic analysis

Eleven thin sections were prepared from samples 1.1, 6.2, 8, 11, 13.1, 14.2, 16, 20, 20.1, 28.1 and 35.1 collected during fieldwork. Sample locations are found on the overview map (Figure 1). The thin sections were prepared to the standard thickness of 30µm; however, section 20.1 was visibly thicker than standard, affecting its

interference colours and limiting petrographic interpretation. Thin sections were examined under plane-polarised (PPL) and cross-polarised light (XPL).

The thin sections were examined for mineral composition, grain size, alteration phases, reaction textures (e.g. zoning, corona textures, resorption), grain-boundary relationships, and mineral overgrowths. Modal proportions were visually estimated for selected sections; no systematic point counting was undertaken.

3.4 SEM analysis

Carbon-coated thin sections 14.2, 20.1, 28.1 and 35.1, together with a small residual rock fragment from sample 50, were analysed at the Swedish Museum of Natural History using a FEI Quanta field-emission SEM equipped with an 80mm² X-MaxN Oxford Instruments EDS detector, operated at 20 kV with a working distance of 10mm. The beam current was calibrated on Co metal, and the instrument was calibrated against metal and mineral standards for each element.

Preparation of sample 50 as a conventional 30µm thin section was unsuccessful, and only a thin sliver remained. The exposed surface was manually polished by the SEM operator. The results from sample 50 were therefore interpreted with caution.

SEM-EDS analyses focused on identifying mineral phases and determining mineral compositions. The chemical compositions of mineral spot analyses were acquired and processed using Oxford Instruments AZtec software with a standard ZAF matrix correction.

4 RESULTS

The maps below show the observed lithologies of Östra Lagnö. Figure 1 provides an overview of the investigated field sites and locations of samples taken for thin section. Figure 2 to Figure 4 show detailed lithologies and features.

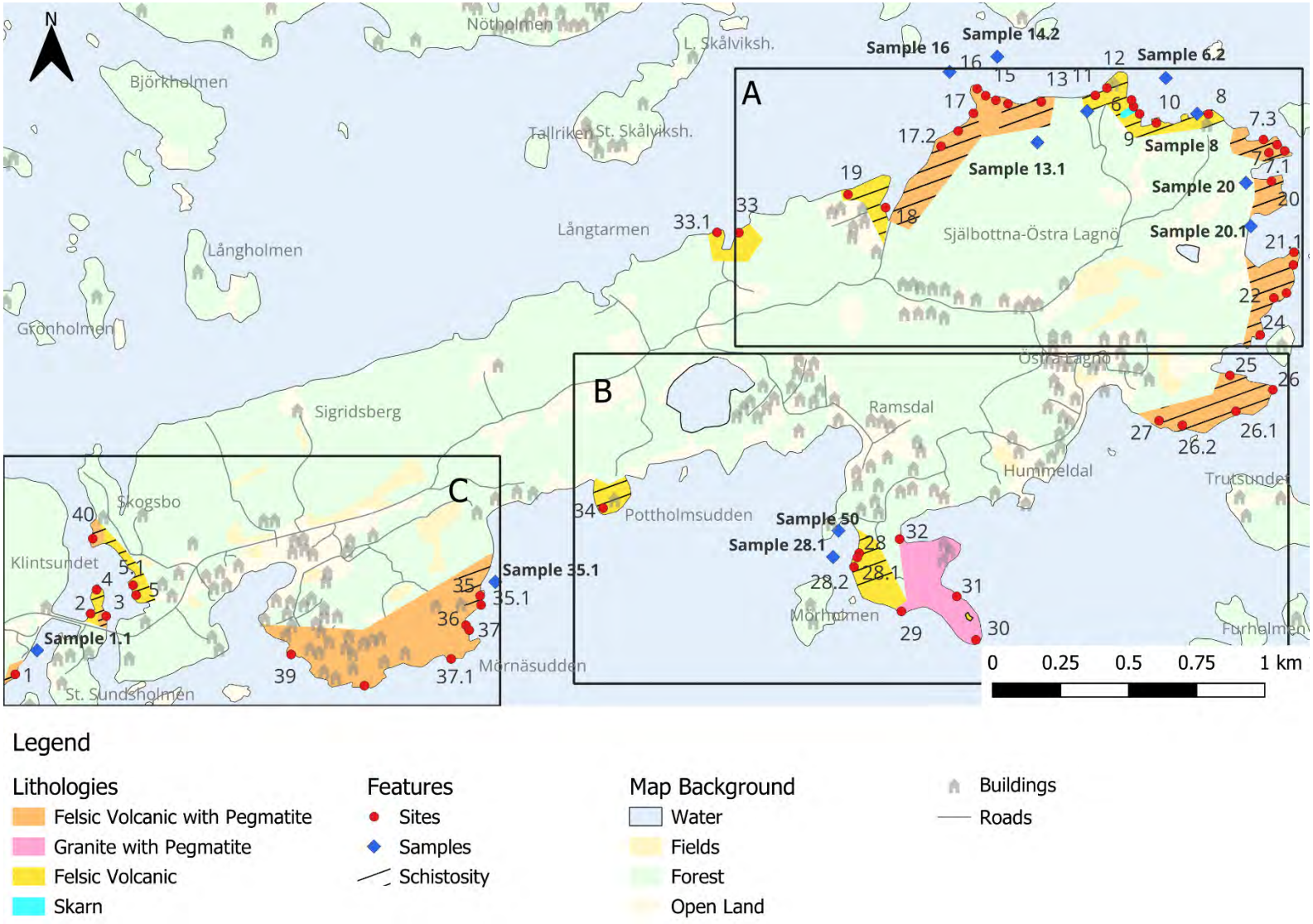


Figure 1. Geological overview map of Östra Lagnö, Stockholm region, Sweden. Boxes A-C mark the sections shown in detail in Figures 2-4.

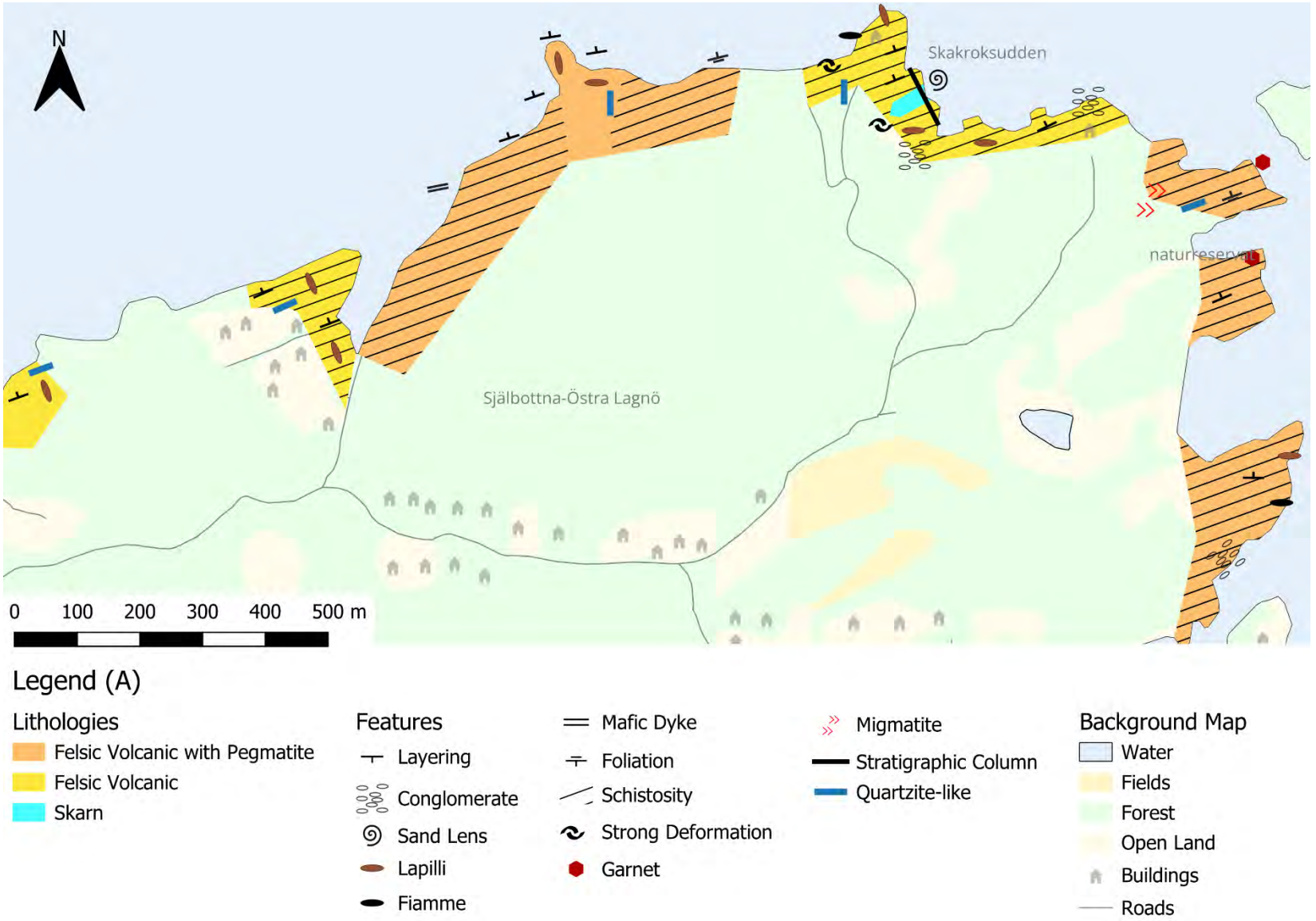


Figure 2. Detailed geological map of section A.

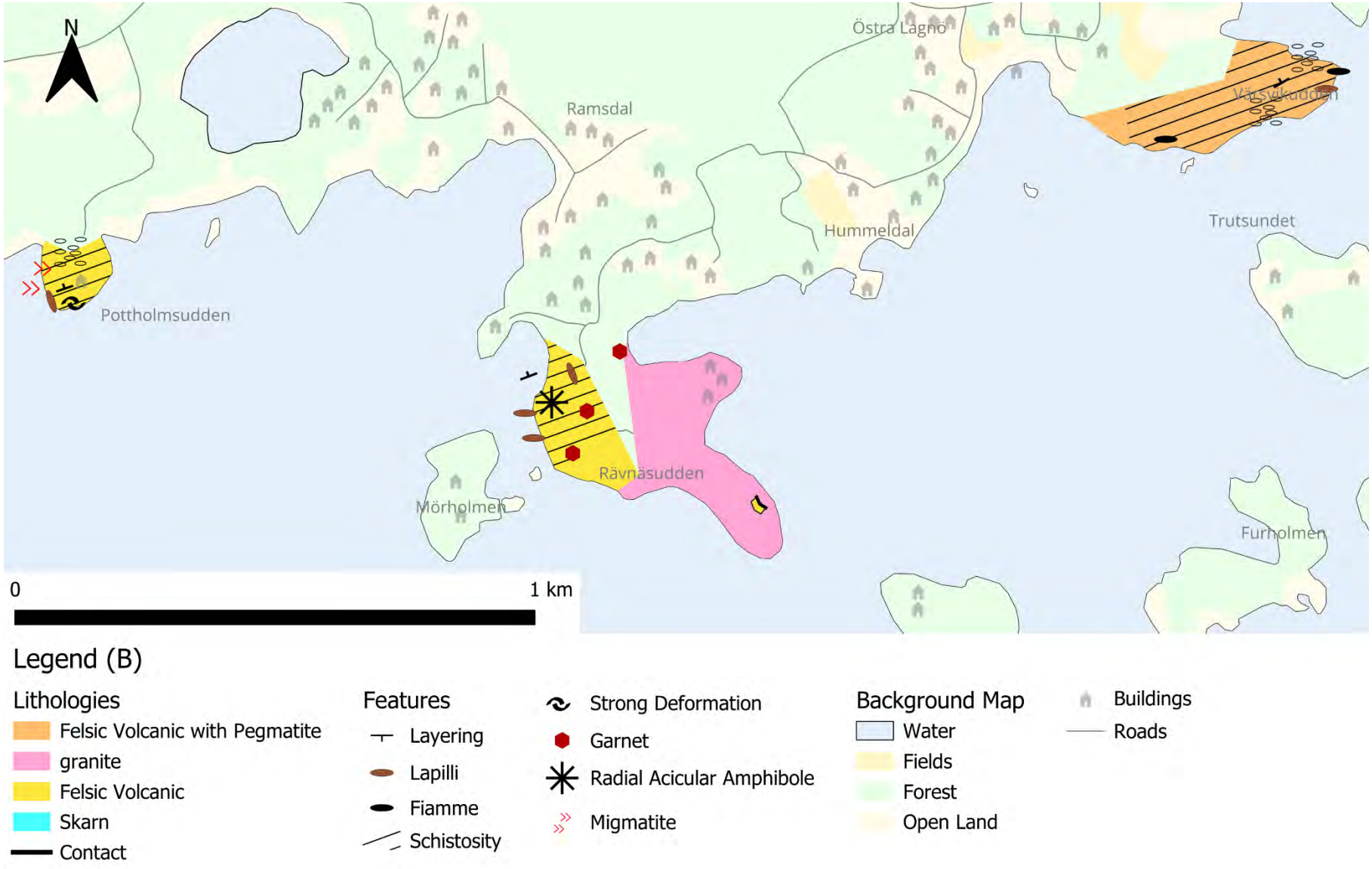


Figure 3. Detailed geological map of section B.

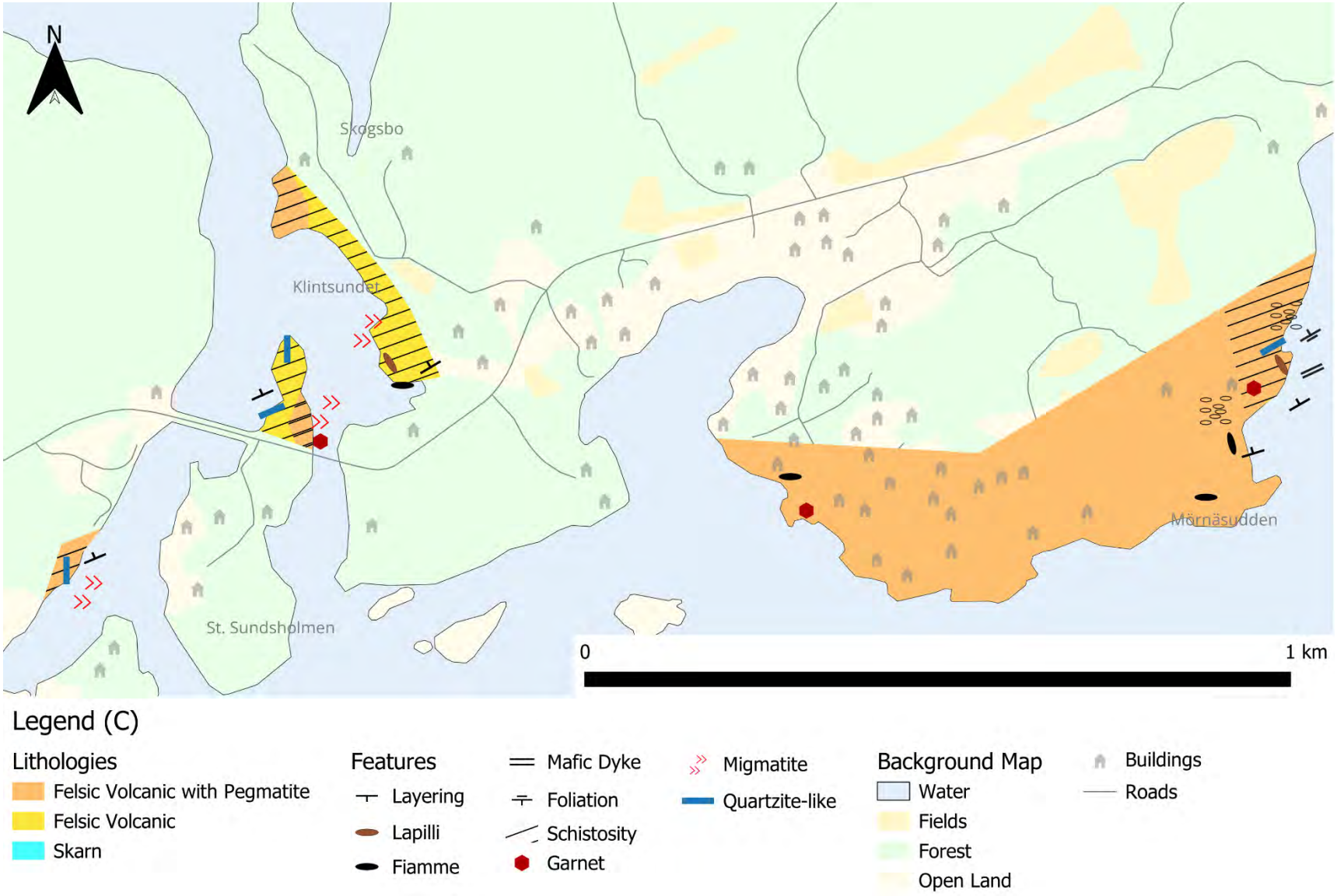


Figure 4. Detailed geological map of section C.

4.1 Felsic volcanic rocks



Figure 5. Finely laminated, ash-like layers in felsic metavolcanic rock at Site 6. Compass for scale.

The dominant lithology on Östra Lagnö is categorised as felsic metavolcanic rock. It occurs throughout the mapped area. It is generally hard and resistant to weathering, and ranges from beige to dark grey. Grain sizes and textures vary. There are fine-grained laminated varieties of ash-sized grains (Figure 5), coarser-grained layered units with sand-sized grains containing modified volcanic fragments and fiamme, and massive, homogeneous ignimbrite-like units with elongated lapilli and aligned fiamme (Figure 6). At Site 26, the outcrop of this unit is especially large and continuous at approximately 200 metres length and 100 metres width. Transitional types also occur. The principal field characteristics of representative sites are summarised in Appendix Table F.



Figure 6. Massive felsic metavolcanic unit containing elongated lapilli and dark, flattened features, possible fiamme. Hand lens for scale.

In thin section, lapilli show as rounded, recrystallised domains (Figure 7).

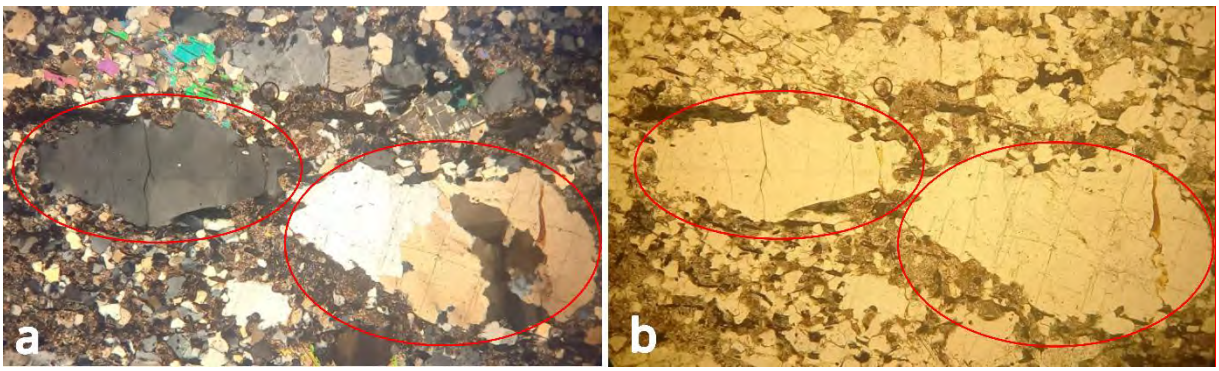


Figure 7. XPL (a) and PPL (b) photomicrographs of the same field of view in Sample 8, showing two rounded, quartz-filled domains (outlined in red) within a finer-grained matrix. Magnification not recorded.

Throughout the mapped area, quartzite-like felsic units with coarse grain sizes also occur. Some are banded with darker, finer-grained ash (Figure 8). The units can contain lapilli and fiamme, and abundant, large, angular plagioclase crystals are visible in thin section. The term “quartzite” in this study is used only descriptively to indicate their grain size (sand-sized) and recrystallisation texture.



Figure 8. Quartzite-like felsic volcanic unit at Site 35. Hand lens for scale.

The felsic volcanic rocks occur in various relationships with other rock types, such as pegmatite, mafic material, and a mapped contact with a possible grantitic pluton at Site 31 (Section 4.4).

The field categorisation of the samples described in this section as felsic volcanic was supported by petrographic examination. The examination of thin sections 1.1, 8, 11 (Site 12), 13.1, 16, 20, 28.1, and 35.1 revealed quartz-feldspar-rich assemblages with abundant, large plagioclase grains, and variable proportions of muscovite, biotite, and chlorite. Mica content is high relative to quartz and feldspar in several samples. Sample 50 is excluded, as it was only examined by SEM-EDS. Fine-grained sericite occurs throughout this sample group as a common feldspar-alteration texture. Additional phases included garnet, amphibole, and epidote, together with accessory minerals such as apatite, zircon, and opaques. The principal mineralogies, textures, and estimated modal proportions, are summarised in Appendix Tables EMP and AM.

4.2 Mafic rocks



Figure 9. Two parallel mafic bands (dark, above and below the scale) within the felsic host rock at Site 9. Folding ruler (~2m) for scale.

Mafic material occurs predominantly as narrow bands or tabular bodies within the felsic volcanic lithology. These units are generally dark and fine-grained (typically ≤1mm) and range from homogeneous and massive to distinctly schistose (Appendix Table M).

Sample 14.2 was collected from mafic material at Site 14. The thin section is biotite-dominated and displays a schistose fabric with preferentially aligned biotite. The visual modal estimate was approximately 40-50% biotite with subordinate amphibole, quartz, and feldspar.

4.3 Possible sedimentary and volcaniclastic units

Sedimentary-looking units occur throughout the map. They resemble the quartzite-like units described in Section 4.1. Due to limited sampling, it was not possible to distinguish between primary sedimentary and volcanic units of this type. All sampled “quartzite-like” rocks showed volcanic features.

Conglomerate-like units occur locally as discrete layers within the felsic lithologies. These units contain abundant clasts of variable composition and size, with poorly sorted particles ranging from gravel-sized material to larger clasts of 10cm, all of which are modified (elongated and showing a preferred orientation).



Figure 10. A layer of poorly sorted, elongated clasts in a fine-grained matrix at Site 22. Folding ruler for scale.

Additional possible sedimentary depositional features are locally preserved. At Site 6, coarser sand-rich layers and two lens-like features occur interlayered with fine-grained, laminated material. At Sites 7.1 and 7.3, possible graded bedding was identified, but younging could not be established due to vegetation cover.



Figure 11. Pale, lens-shaped, coarser-grained feature within darker, fine-grained rock at Site 6.1. Folding ruler for scale.

Calc-silicate or skarn-like units were observed at Sites 6-9, to the north-east of the island. They show irregular, pitted weathering surfaces, suggestive of carbonate dissolution and contain epidote visible in the field. The

most substantial occurrence was recorded at Site 6, where it forms a unit at least 5 m long and 1.5 m wide within a layered felsic succession (Figure 12). These units and their contacts are recorded in the sedimentary log (Figure 13). Thin section Sample 6.2 taken from this location shows compositional banding and contains amphibole with epidote.



Figure 12. Skarn exposure at Site 6.2. Folding ruler for scale.

A stratigraphic log was recorded from Sites 6-9. The upper part of the measured section (Figure 13) is dominated by laminated fine ash, interrupted by two beds of sand-rich material and a skarn unit (Section 4.3). Below the water-covered gap, interbedded sand-rich units and a second skarn-bearing unit give way to thick, internally homogeneous coarse ash with an ignimbrite-like character at the base, cut by two thin mafic units.

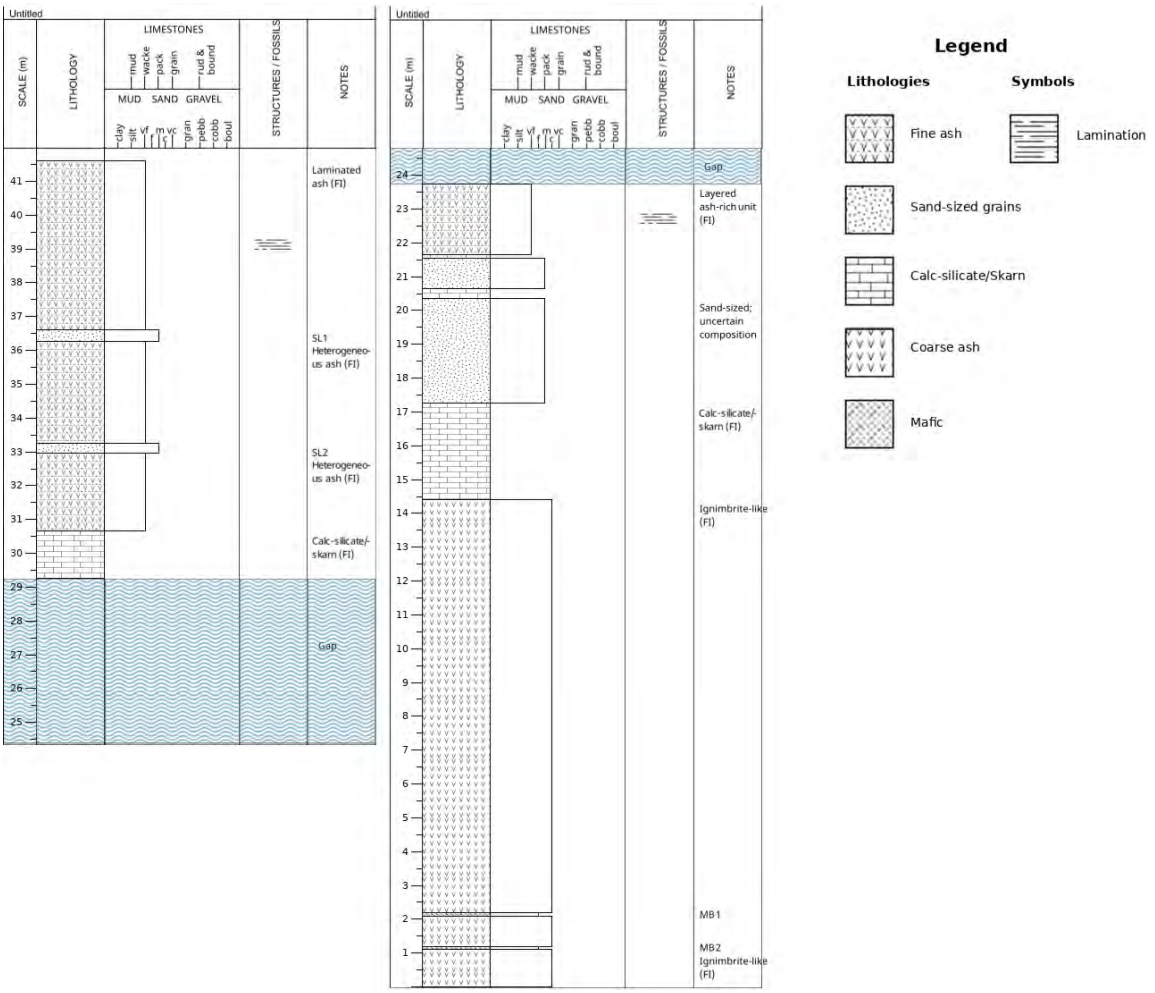


Figure 13. Stratigraphy log Site 6-9. 41.6m with a 5.5m water-covered gap. MB = Mafic Band. FI = Field Interpretation. SL = Sand Lens. Log created in SegLog 3.1 and modified. Younging after Lundqvist (1962); top = NE.

4.4 Intrusive felsic rocks

Granitoids occur primarily around Sites 29-32 in the south of the island. They are generally coarse-grained and quartz-feldspar-rich. Grain sizes exceed 2mm at Site 29 and reach 5mm to 1cm at Site 31. The granitoids are extensively intruded by pegmatite, and an approximately 2-4 m-long section of a contact between granitoid and felsic volcanic rocks is exposed between Sites 30 and 31. This is shown on the geological map section B (Figure 3).

Pegmatite (Figure 14) is widespread across Östra. It is quartz- and feldspar-rich and contains abundant muscovite mica. Garnet occurs in some pegmatites (Section 4.7.1).



Figure 14. Folded pegmatite within strongly schistose host rock at Site 7.2. The folded band reaches approximately 70cm in thickness at its widest point (arrowed).

The pegmatites range from relatively narrow veins (a few centimetres) to very large bodies 10-20 m wide. They commonly cross-cut the felsic volcanic lithologies, and across Sites 29-32 intrude into the granitoid. At several localities, more than one generation of pegmatite is found, with deformed pegmatite cross-cut by younger and less deformed pegmatite. This is clearest at Site 21.1, where two intersecting pegmatite dykes were observed.

The degree of deformation associated with the pegmatites varies. At some localities, the pegmatite appears relatively undeformed, while deformation is concentrated in the surrounding host rock or along pegmatite margins. At Site 31, deformed dark zones occur within the granitoid along parts of the granite-pegmatite contact, while the pegmatite itself appears comparatively undeformed.



Figure 15. Coarse-grained pink quartz-feldspar pegmatite intruding finer-grained granitoid at Site 31, with a dark band developed along part of the contact. Hand lens for scale.

Migmatite- and leucosome-like textures were observed at several localities within the felsic metavolcanic succession. Quartz veins also cross-cut the felsic metavolcanic rocks.

4.5 Structural observations

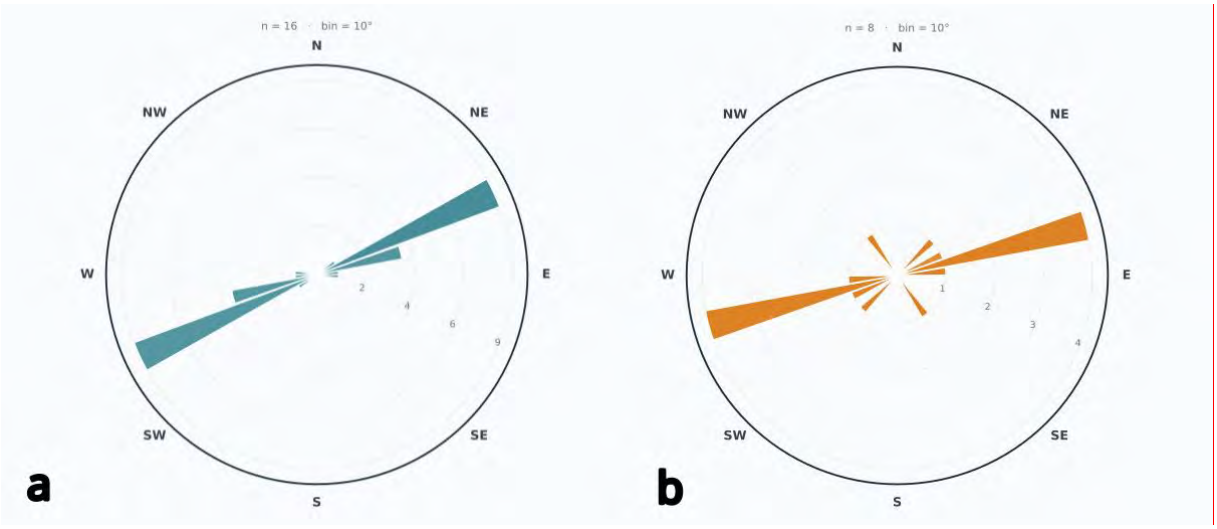


Figure 16. Rose diagrams of structural orientation data from the mapped area. ***a)*** *Strike of compositional/lithological layering (n = 16);* ***b)*** *Strike of foliation (n = 8). Petal length is proportional to the number of measurements per 10° bin.*

Structural features are variably developed across the mapped area. Orientation measurements are summarised in Figure 16 and Appendix Tables SM-A and SM-B. These measurements require caution, as aligned clasts and fiamme may record primary depositional fabrics, later tectonic deformation, or both, and were therefore not treated as unambiguous foliation measurements. The most divergent measurements are the fabric at Site 7.2 (040/84° S) and aligned clasts at Site 22 (145/15° N). Site 37 preserves compositional layering at 073/60° N in felsic volcanic rock showing little visible deformation.

Visible deformation is heterogeneous across the mapped area. Boudinage occurs at several localities and varies in scale, from centimetre-scale structures to metre-scale boudins at Sites 11 and 34. Folding is widespread and affects both the supracrustal rocks and pegmatite bodies. At Site 34, folding, boudinage, schistosity and elongated fragment-like features occur within the same outcrop.



Figure 17. Boudinaged pale felsic material within darker, foliated host rock. Folding ruler (~176cm) for scale.

Schistosity is widely developed but varies in intensity and continuity among outcrops. It is particularly evident at Sites 13, 17.1, 18, 19, 20, 34, 35.1 and 36.



Figure 18. Two schistose, possibly mafic bands adjacent to felsic volcanic rock: a narrow band on the left and a wider band on the right. Folding ruler (~110cm) for scale.

At Site 29, linear surface features measured at 148/39° W represent glacial striations and were therefore excluded from the structural orientation analysis. A possible shear zone was identified between Sites 20.1 and 21.1.

4.6 Site 28 / Rävnäsudden

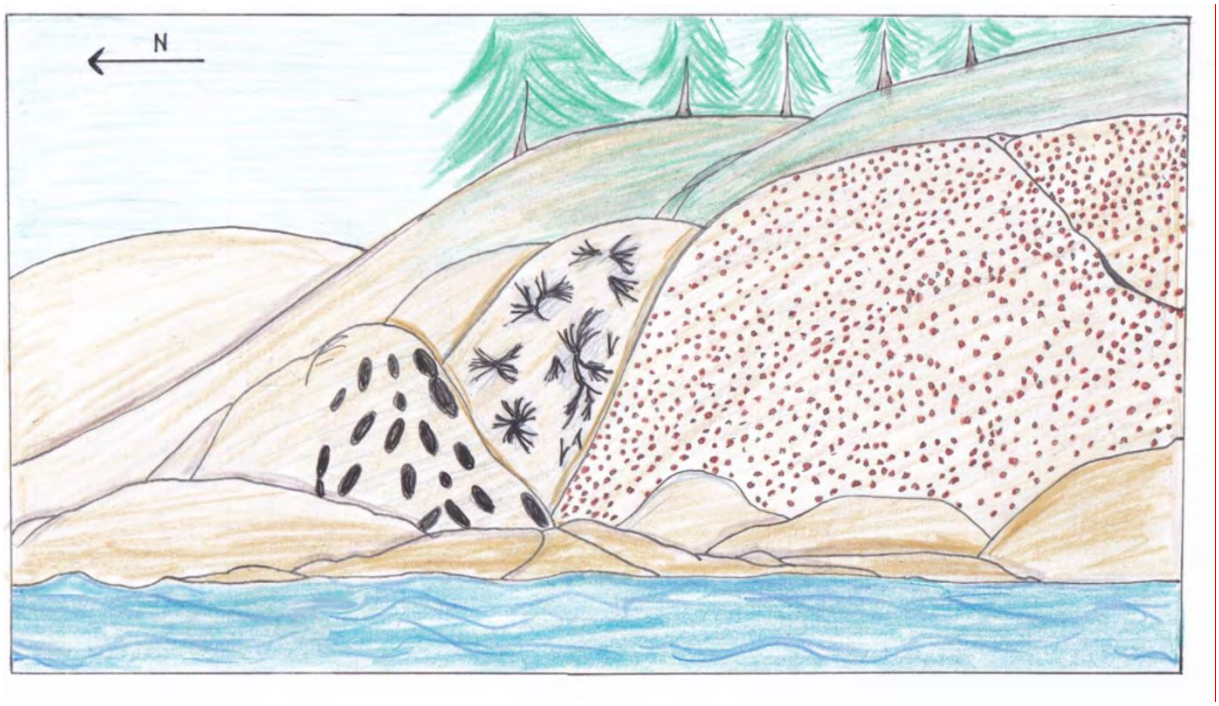


Figure 19. Representative sketch of Site 28. Left: unit containing "egg-shaped" nodules. Middle: radial acicular amphibole. Right: garnet-bearing felsic-volcanic unit. Not to scale.

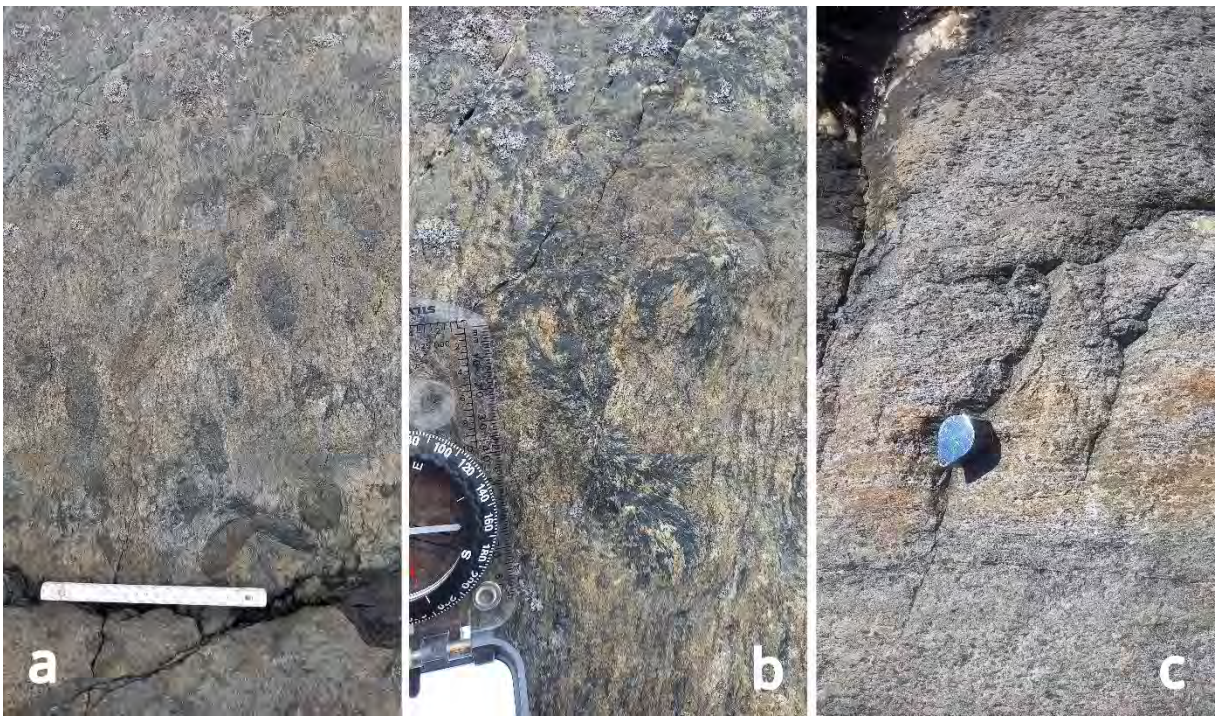


Figure 20. ***a)*** *Ovoid nodules. Folding ruler for scale.* ***b)*** *Radial acicular amphibole. Compass for scale.* ***c)*** *Abundant garnet porphyroblasts in schistose felsic volcanic host rock at Site 28. Hand lens for scale.*

Site 28 / Rävnäsudden is a particular point of interest. At Site 28.2, a distinct amphibole-rich section 1 m wide and 2 m long occurs within the broader felsic volcanic outcrop. The section contains abundant dark amphibole, locally forming radial aggregates 4-7cm in diameter (Figure 20b). Immediately to the north of the amphibole-rich section, unidentified 7-10cm long ovoid features occur in a unit that resembles conglomerate (Figure 20a). Immediately to the south of the amphibole-rich unit sits a felsic volcanic rock bearing abundant garnet (Figure 20c).

4.7 Mineralogical observations

Quartz and feldspars are widespread in the investigated lithologies and have been described in the preceding sections. Compositional data for plagioclase and alkali feldspar, obtained by SEM-EDS, are presented below.

Accessory minerals are common, but were not investigated in sufficient detail to constrain protolith, metamorphic grade or mineral origin, and they are not discussed further. They are listed in Appendix (AM).

The full chemical data on which the ternary diagrams are based can be found in the Appendix.

4.7.1 Garnet

Garnet is the most conspicuous metamorphic mineral recorded in the mapped area and occurs in more than one lithological setting. At Sites 28.1 and 35.1, garnets are particularly abundant in the felsic volcanic host rock and mostly 1mm in diameter, with some reaching 5mm, and at Site 28.1 pale zones around clusters of garnet exist in the host rock (Figure 21).



Figure 21. Pale patches surrounding garnet at Site 28.1. Hand lens (~5cm) for scale. Photo:Joakim Mansfeld.

Garnet occurs in some pegmatites in varying quantities and sizes (<1mm-5mm), and the garnets in pegmatite Sample 20.1 differ texturally and chemically from garnet in the non-pegmatitic felsic volcanic host rock. They are largely euhedral (Figure 22) and their chemistry is more Mn-rich than garnet in the felsic volcanic host rock.

In the felsic volcanic lithology, garnets are either euhedral and well preserved or strongly weathered with breakdown textures and cracks (Figure 22). In Samples 28.1 and 35.1, some garnet overgrows the biotite-defined foliation (Figure 22a), and shows poikiloblastic texture with quartz inclusions. Specific garnet occurrences are wrapped by a sheet silicate optically resembling biotite or chlorite (Figure 22f and d). SEM-EDS analysis of this phase yielded very low K together with Si, Al, Fe, and Mg, but also appreciable Na and Ca, (Table 1) and may represent a mixed composition, possibly including adjacent plagioclase. Some fractured garnet crystals locally contain possible chlorite (in places intergrown with mica) within the cracks, and embayment

textures are visible in some garnets (Figure 22e).

Table 1. SEM-EDS oxide composition of the sheet-silicate material next to garnet in Sample 28.1.

Oxide	Wt%	Atomic %	Cations per 11 O	Cations per 14 O
Na_2O	2.83	2.27	0.400	0.509
MgO	2.11	1.30	0.229	0.292
Al_2O_3	15.59	7.59	1.338	1.703
SiO_2	53.86	22.25	3.922	4.991
K_2O	0.56	0.30	0.053	0.067
CaO	4.59	2.03	0.358	0.455
TiO_2	0.23	0.07	0.012	0.016
FeO	5.14	1.78	0.314	0.399
Total	84.91	37.59	6.625	8.432

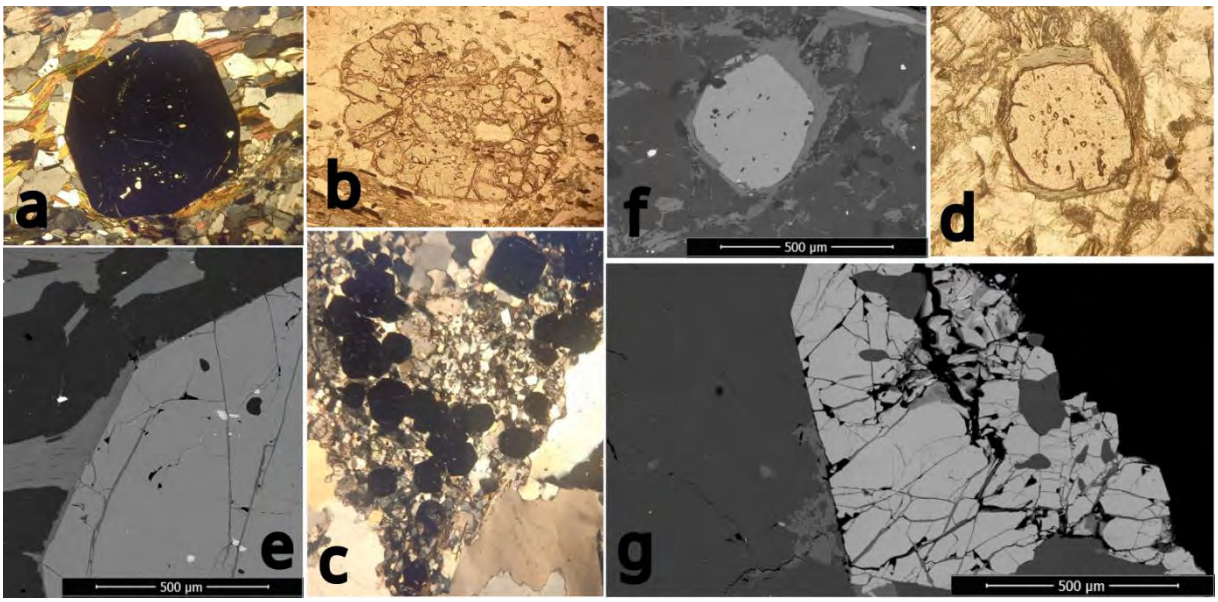


Figure 22. Thin section and SEM photographs of garnets. Magnification not recorded for thin sections. ***a)*** *Euhedral poikiloblastic garnet surrounded by biotite in Sample 35.1. Thin section.* ***b)*** *Fractured garnet in Sample 28.1. Thin section.* ***c)*** *Sub- to euhedral garnets in Sample 28.1. Thin section.* ***d)*** *Biotite, chlorite, or a mixed phase wrapping around garnet in Sample 28.1. Thin section.* ***e)*** *Garnet with embayed edges in Sample 35.1. SEM.* ***f)*** *Biotite, chlorite, or a mixed phase wrapping around garnet in Sample 28.1. SEM.* ***g)*** *Preserved straight edges in garnet Sample 20.1. Fractures possibly a result of thin section manufacturing. SEM.*

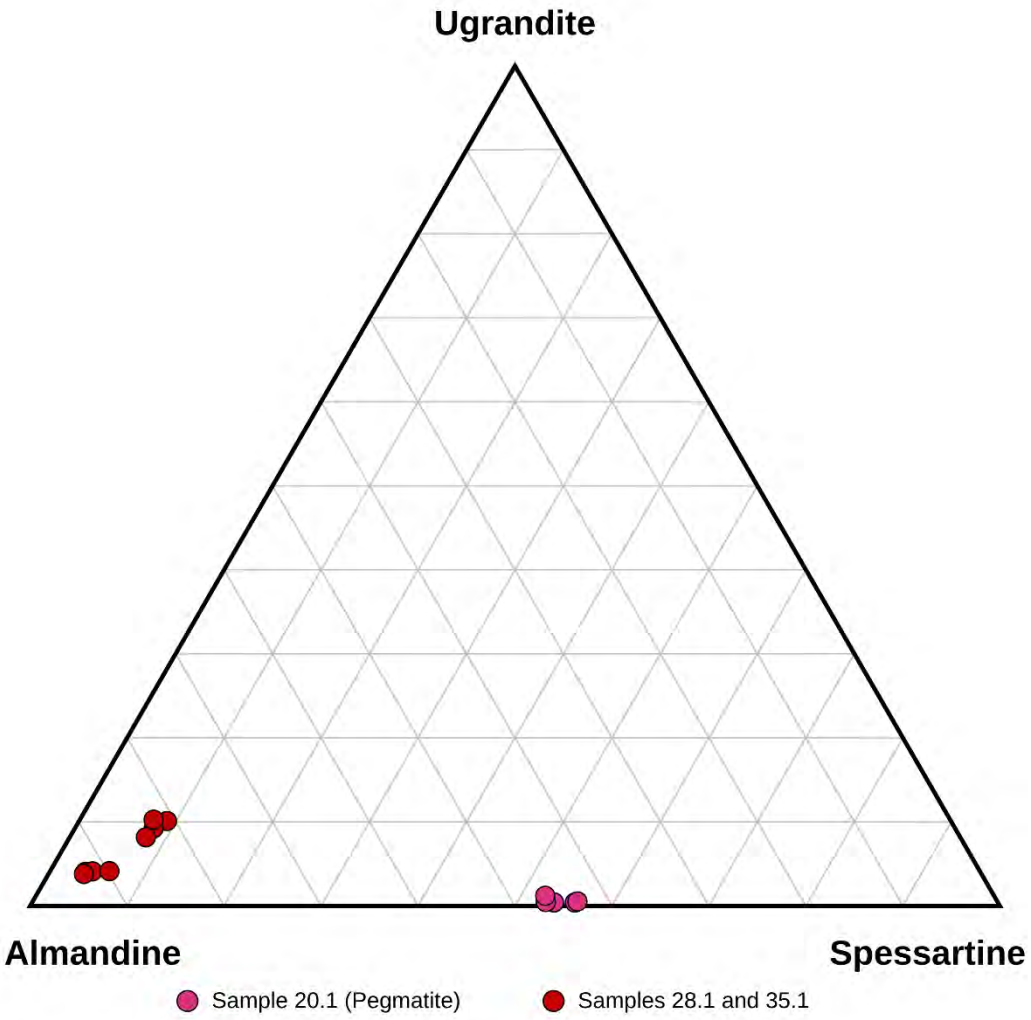


Figure 23. Spessartine-Almandine-Ca-garnet ternary diagram (Ca-Fe-Mn), for garnet analyses from Samples 20.1, 28.1, and 35.1. Mg is excluded from this normalisation. Full SEM analysis tables in Appendix 0.

All 13 garnet analyses plot along the Almandine-Spessartine join, with a minor Ugrandite (Ca-garnet) component. Two compositional groups are present: Samples 28.1 and 35.1 cluster near the Almandine corner, while five points from Sample 20.1 plot toward the Spessartine corner.

4.7.2 Amphiboles

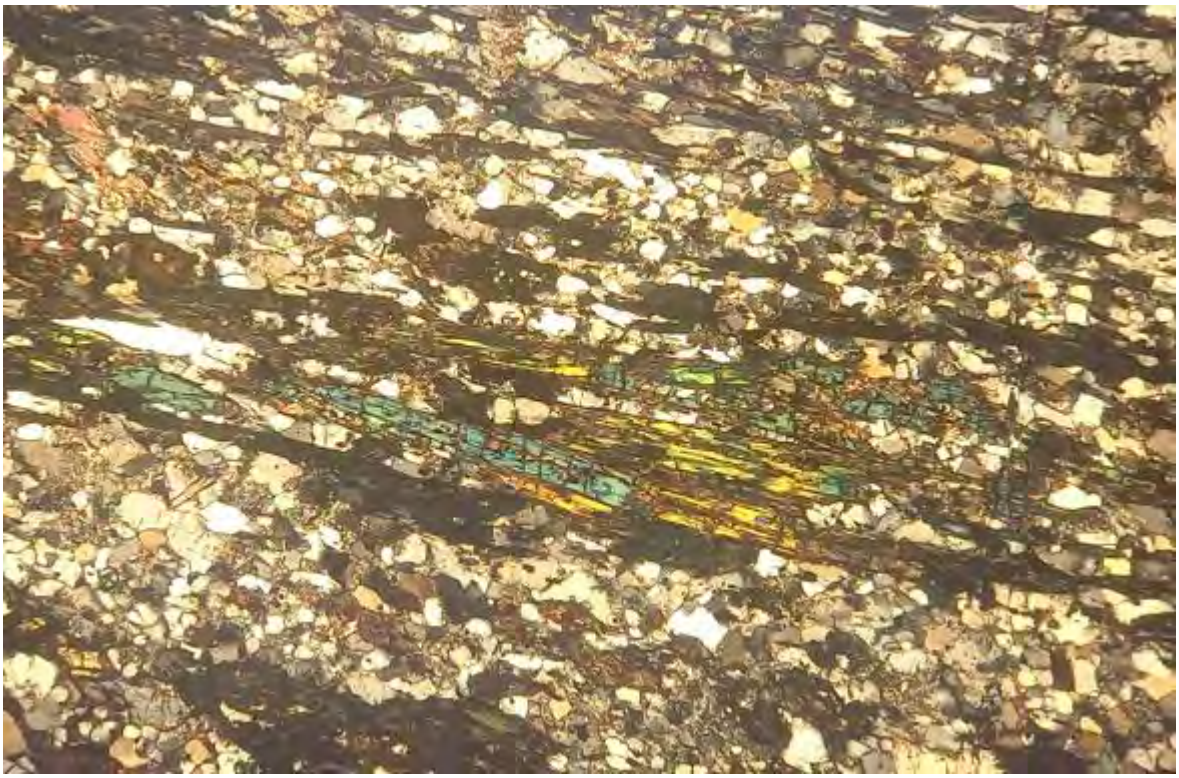


Figure 24. Acicular pargasite in thin section 28.1. The amphibole is aligned with the metamorphic fabric. Magnification not recorded.

Amphiboles occur as another important metamorphic mineral phase locally. They were identified in Samples 6.2, 14.2, and 28.1. Fe^{3+} could not be determined by SEM-EDS; all Fe is assumed to be Fe^{2+}

SEM-EDS analyses of amphibole in Sample 28.1 define two compositionally distinct groups. Analyses 12 and 17 are Ca- and Al-poor Fe-Mg amphiboles compatible with the cummingtonite-grunerite/anthophyllite group, while analyses 9 and 21 are Al-Na-rich calcic amphiboles classified as pargasite in accordance with Hawthorne et al. (2012). The pargasite is acicular, aligned with the foliation, and locally overgrows it.

In Sample 14.2, a dark green to dark brown amphibole was optically identified as hornblende, and individual amphibole crystals locally occur across or overgrow the aligned biotite fabric. Five SEM-EDS analyses of amphibole crystals, with A-site occupancy (Na + K) of 0.48-0.55 apfu, are consistent with pargasite; only point 14.2-7 plots marginally below the pargasite boundary at 0.48 apfu. An additional analysis (point 14.2-23) produced anomalously high Ca and total cation values, possibly reflecting overlap with an adjacent Na-Al-rich phase, and was excluded from the reported compositional range and ternary diagram (Table 2). Full atomic %, oxide wt%, and cation proportion data are provided in Appendix Tables A2a-A2e.

Table 2. SEM-EDS amphibole compositions grouped into Al-Na-(Mg+Fe) cation scheme (Tschermakite-Tremolite/Actinolite-Glaucophane), Samples 14.2 and 28.1.

Sample & Spectrum	Al (cations)	Na (cations)	Mg+Fe (cations)	Cation sum (Al+Na+(Mg+Fe))	Tsch %	TrAct %	Gln %	Included?
14.2-7	2.216	0.275	4.451	6.941	31.9	64.1	4.0	Yes
14.2-20	2.148	0.306	4.454	6.908	31.1	64.5	4.4	Yes
14.2-23	3.190	1.047	4.831	9.069	35.2	53.3	11.6	No
14.2-29	2.183	0.317	4.458	6.958	31.4	64.1	4.6	Yes
14.2-37	2.274	0.325	4.450	7.050	32.3	63.1	4.6	Yes

14.2-38	2.175	0.283	4.529	6.987	31.1	64.8	4.0	Yes
28.1-9	2.678	0.556	4.893	8.127	33.0	60.2	6.8	Yes
28.1-12	0.419	0.000	6.699	7.117	5.9	94.1	0.0	Yes
28.1-17	0.384	0.000	6.752	7.136	5.4	94.6	0.0	Yes
28.1-21	2.769	0.685	4.302	7.756	35.7	55.5	8.8	Yes

In Figure 25, Samples 14.2 and 28.1 are plotted together to show the compositional range of amphibole across the study area. The Sample 6.2 amphibole in the skarn-bearing unit was identified only optically and falls within the actinolite/tremolite to hornblende range. It is therefore not included in the ternary diagram (Figure 25).

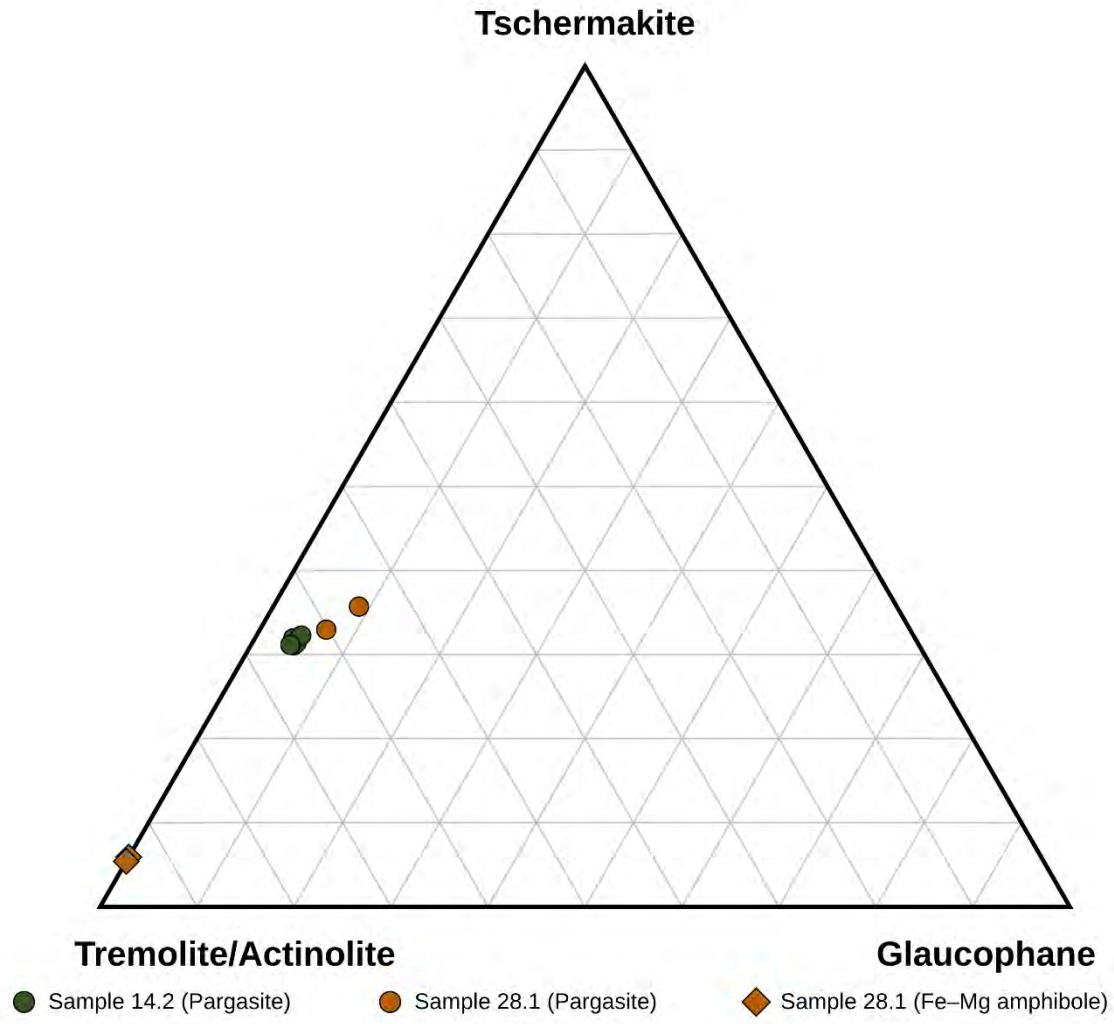


Figure 25. Tschermakite-Tremolite/Actinolite-Glaucophane ternary diagram (23-oxygen basis, calculated on Al, Fe+Mg, and Na). Sample 28.1 contains two compositionally distinct amphiboles: pargasite, which plots with Sample 14.2, and a Ca- and Al-poor Fe-Mg amphibole of cummingtonite-grunerite/anthophyllite type.

Additional hornblende was identified in the field in mafic rocks, where it occurs with biotite and muscovite mica. A radial, sheaf-like amphibole was also observed in the field at Site 28.2 (Figure 20b) but was not sampled for analysis. It is texturally distinct from the amphibole in Sample 28.1 and shows no deformation.

4.8 Other minerals

Plagioclase commonly occurs as relatively unaltered grains, larger than the surrounding groundmass. SEM-EDS

analyses of feldspar from Samples 14.2, 20.1, 28.1, 35.1 and 50 are shown in Figure 26.

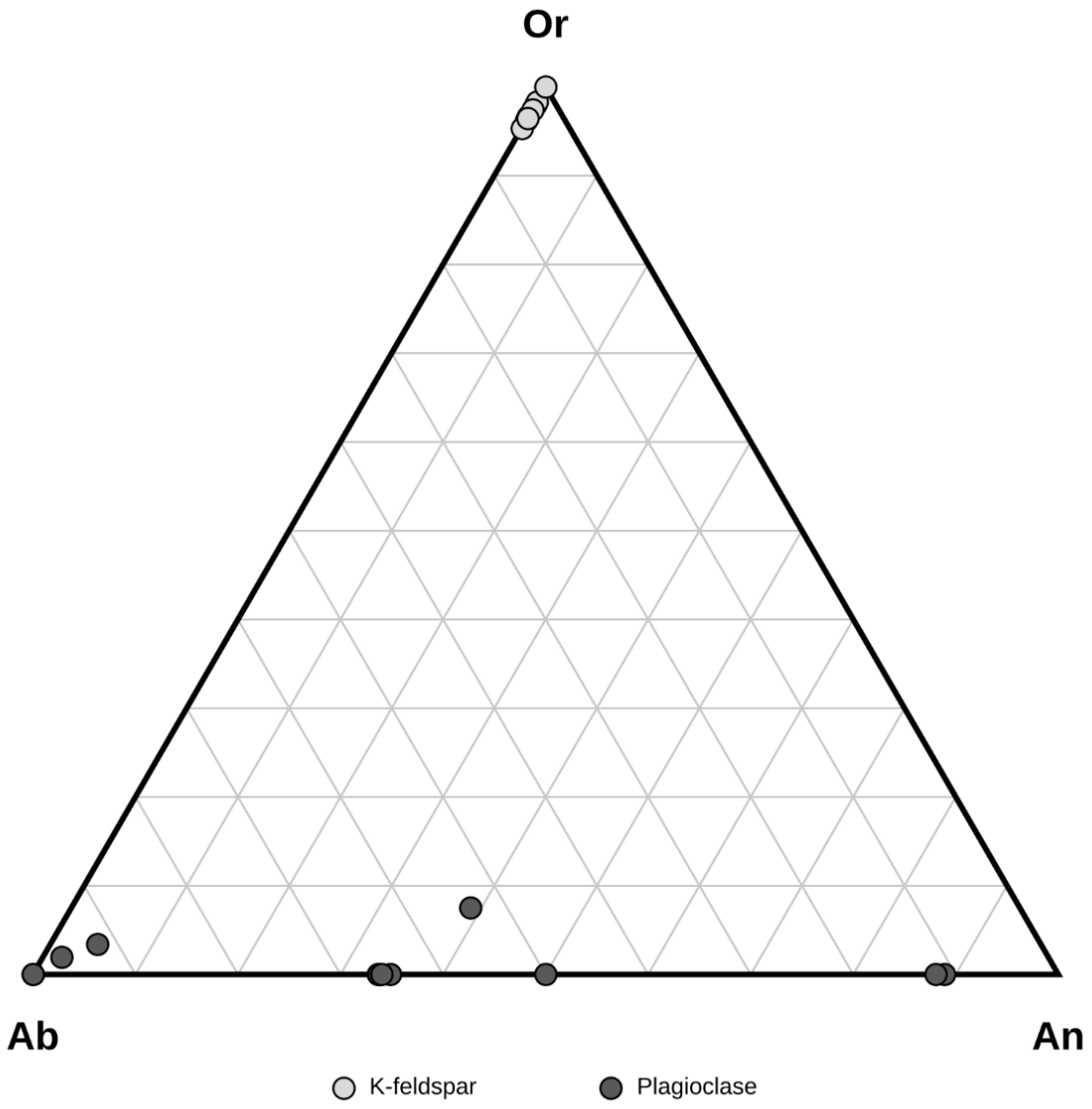


Figure 26. Albite-Anorthite-Orthoclase (Ab-An-Or) ternary diagram (8-oxygen basis) for plagioclase and alkali feldspar analyses across all studied samples.

Sample 14.2 contains two plagioclase compositions, bytownite (An88-89) and albite (Ab100), each represented by two analyses; all four have low totals (~80-90 wt%) but acceptable stoichiometry, and alkali feldspar is also present. Plagioclase in Samples 28.1 and 35.1 is andesine (An34-50), and in Sample 50 it is albite. Sample 20.1 yielded only alkali feldspar.

Biotite and muscovite are widespread and are particularly common in schistose lithologies (Appendix Table EMP). Most mica grains appear optically fresh, although local alteration and replacement textures occur. In several samples, individual mica grains overgrow the granoblastic quartz-feldspar fabric, and some display poikiloblastic inclusions of quartz. Chloritisation is particularly evident in Sample 28.1, ranging from partial replacement of individual mica grains to chloritised mica-rich domains. Chlorite also occurs in other samples in association with mica minerals.

Epidote-group minerals occur in Samples 6.2, 14.2, 16, 28.1 and 50. In Sample 6.2, epidote occurs within the fine-grained quartz-plagioclase matrix together with acicular amphibole (actinolite/tremolite). In Sample 14.2, SEM-EDS identified clinozoisite/epidote, and some epidote-group minerals overgrow the biotite fabric. In Sample 16, epidote forms a square-shaped rim around a possible pyroxene, although the identity of the enclosed mineral could not be confirmed.

5 DISCUSSION

5.1 Geological succession and depositional history

Though primary textures have been extensively recrystallised throughout the study area, the dominant lithology is interpreted to have originated as felsic volcanic and volcaniclastic deposits. This interpretation is supported by the preservation of fiamme, lapilli, ash-rich layers, and finer-grained laminations, locally fragmental or ignimbrite textures, and by the presence of abundant plagioclase crystals interpreted as pheno- or xenocrysts.

The massive units containing lapilli and fiamme are interpreted as ignimbrite, and the finely laminated units as ash-fall deposits. The fiamme are oriented within the dominant foliation (Section 4.5) and do not show the discordant fiamme foliation that Allen et al. (1996) use to distinguish primary from tectonic fabrics in Bergslagen, so tectonic flattening cannot be excluded.

The high mica content in some samples could suggest a pelitic protolith, but is here interpreted to reflect hydrothermal alteration of feldspar in originally volcanic material, producing sericite that coarsened to mica during metamorphism.

At Rävnäsudden (Site 28), the ovoid do not correspond well to the conglomeratic clasts of mafic composition described by Lundqvist (1962). They display reddish-brown surface patches and lack a consistent preferred orientation, which is more consistent with in-situ growth than with deformed sedimentary clasts. Their size is large for individual cordierite porphyroblasts, but their brownish weathering is consistent with pinite after cordierite, as reported by Lundqvist (1962) in this area. The amphibole-rich section at Site 28.2 is interpreted as felsic volcanic rock modified by Mg-metasomatism rather than a primary mafic rock (Section 4.7). The radial amphibole at Site 28 is undeformed (Figure 20b), indicating growth after the main deformation event, consistent with Lundqvist's (1962) interpretation of post-deformational magnesia metasomatism. The lithological variation at Rävnäsudden therefore reflects post-depositional alteration of felsic volcanic rock.

The locally quartz-rich ("quartzite-like") rocks with sand-sized grains, interbedded locally with laminated ash-rich material, contain abundant plagioclase compatible with a volcanic protolith, indicating reworking of volcaniclastic material rather than purely epiclastic deposition. Grading at Sites 7.1 and 7.3 supports reworking. The polymict conglomeratic units also record incorporation and redeposition of previously formed material. However, some lens-shaped fragments aligned with layering may represent disrupted segments of originally continuous layers rather than primary clasts.

The fine lamination preserved at Site 6 and elsewhere records suspension settling in a low-energy subaqueous environment. The skarn-bearing unit is interpreted to have developed from a layered, carbonate-rich precursor, consistent with the compositional banding preserved within the unit and the karst-like weathering observed in the field.

Taken together, the succession records repeated felsic volcanic and volcaniclastic deposition with local sedimentary or reworked material in a subaqueous setting.

5.1.1 Regional depositional context

The geology mapped in this study broadly matches Lundqvist's (1962) description of Östra Lagnö. The mapped area is dominated by felsic supracrustal rocks corresponding to Lundqvist's "leptites" and dacitic metatuff(ites), together with subordinate mafic to intermediate rocks, carbonate- and skarn-bearing rocks, granitoids, and younger pegmatite dykes.

The present study allows some of Lundqvist's "leptites" to be more specifically interpreted as felsic metavolcanic and metavolcaniclastic rocks on the basis of preserved primary textures. Lundqvist (1962) also reported conglomerates and graded bedding on Östra Lagnö. At Rävnäsudden, (Site 28), he used conglomerate clast composition in interpreting the stratigraphic succession. The polymict conglomeratic units identified in the present study provide broadly comparable observations.

Lundqvist's proposed northward younging direction could not be verified. His reported graded bedding near Site 39 is no longer accessible. Given that Gavelin et al. (1976) documented changes in facing associated with folding at Utö, the present orientation of any grading does not necessarily represent the original younging

direction.

Comparison with Utö provides a useful regional analogue (Gavelin et al., 1976), as both areas contain felsic volcanic or volcaniclastic rocks associated with sedimentary or reworked material, mafic lithologies, and carbonate- or skarn-bearing rocks. Allen et al. (1996) and Talbot (2008) describe shallow-water sands and storm-reworked lenses associated with pyroclastic deposits on Utö, providing a regional context for the sand-rich and lens-like units on Östra Lagnö. These similarities support sedimentary reworking within a comparable volcanic-sedimentary basin setting.

Talbot (2008) also described subaqueous mass-transport deposits on Utö. These provide a regional process analogue for the secondary transport and redeposition recorded by the conglomeratic and finely laminated units on Östra Lagnö.

Important differences nevertheless prevent direct stratigraphic equivalence. The Utö hälleflinta-leptite succession contains substantially more limestone and skarn, as well as iron formation and sulphide mineralisation (Gavelin et al., 1976), whereas these features are absent or only locally developed in the mapped Östra Lagnö succession. The graded turbidites, channel conglomerates, and cross-bedded shallow-water sands described from Utö (Talbot, 2008) were not observed on Östra Lagnö. Gavelin et al. (1976) correlated the south-eastern Utö metasediment group with Lundqvist's lowermost 'oldest leptites' (interpreted as metamorphosed greywackes), and the Utö hälleflinta-leptite group, with its limestones and iron ore, with the uppermost limestone-bearing leptites in Lundqvist's succession. On this basis, the Östra Lagnö rocks may correspond to the lower-to-middle part of the Utö succession; shared depositional processes do not imply equivalent stratigraphy.

At the broader Bergslagen scale, the association of felsic volcanic and volcaniclastic rocks with reworked deposits, local sedimentary material, and carbonate-bearing units is characteristic of Palaeoproterozoic supracrustal successions (Allen et al., 1996). Östra Lagnö can therefore be placed within this broader volcanic-sedimentary framework, although the local age relationships are unresolved.

5.2 Minerals and metamorphism

The petrographic evidence for substantial metamorphic modification of the felsic volcanic rocks (Section 4.7) is consistent with their classification as leptites (Lundqvist, 1962)."

Considering the rocks' metamorphic mineral assemblages, garnet provides particularly useful evidence for distinguishing different stages and origins of mineral growth. The overgrowth and poikiloblastic textures of almandine garnet in the felsic volcanic host rock are evidence for growth after development of the biotite-defined foliation.

The garnet clusters and their pale halos at Site 28 (Figure 21) may represent pseudomorphs after cordierite, matching Lundqvist's (1962) report of cordierite at this locality. However, similar pale patches occur in the same rock without garnet, so this interpretation is not confirmed.

In contrast, pegmatite hosts the Mn-rich spessartine end member, and together with its textural features, this composition supports crystallisation of the garnet from the pegmatitic melt. Mn enrichment is commonly characteristic of garnet crystallising from evolved, fractionated pegmatitic melts (Hernández-Filiberto et al., 2021). The compositional difference between the two garnet populations therefore supports distinct origins for the pegmatite-hosted and host rock garnets.

Amphibole occurs in several different lithological and textural settings. In Sample 6.2, the presence of actinolite-tremolite is consistent with the calc-silicate/skarn assemblage. In mafic Sample 14.2 and felsic sample 28.1, pargasite is interpreted as metamorphic. The cummingtonite-grunerite/anthophyllite-compatible compositions in Sample 28.1 are consistent with Lundqvist's (1962) report of anthophyllite and hornblende locally altered to cummingtonite at this locality.

Together with the cordierite reported by Lundqvist (1962) at Rävnäsudden, the garnet- and anthophyllite-bearing assemblage at Site 28 aligns with the cordierite-garnet-anthophyllite-bearing rocks characteristic of altered felsic volcanic successions in Bergslagen, where they are interpreted as metamorphosed products of synvolcanic hydrothermal Mg-alteration (Allen et al., 1996). Lundqvist (1962) instead attributed these assemblages to a post-deformational "magnesia-metasomatism". As cordierite was not found in this study, these interpretations cannot be confirmed without whole rock chemistry.

The contrasting chemistry of the amphiboles therefore reflects the different bulk compositions and alteration histories of the host rocks.

In the calc-silicate/skarn assemblage at Site 6, epidote formed as a metamorphic reaction product within the Ca-rich assemblage, whereas in Sample 28.1 it is interpreted as later fluid-assisted alteration of the metamorphic assemblage. In Sample 14.2, clinozoisite represents metamorphic growth. The epidote-group minerals therefore reflect different reaction histories or environments in the different lithologies.

Aligned biotite and muscovite define the foliation in several samples. Muscovite provides a useful constraint on the thermal history, as it becomes unstable at sufficiently high temperatures in quartz-bearing rocks.

Lundqvist (1962) described andesine-range plagioclase in felsic metavolcaniclastic rocks on Östra Lagnö, and coarse plagioclase crystals within a finer groundmass which he interpreted as phenoclasts. The andesine compositions observed in Samples 28.1 and 35.1 are compatible with both relict magmatic and metamorphic plagioclase. If relict, it would support the interpretation of the larger plagioclase grains as possible pheno- or xenocrysts; if recrystallised, it would reflect re-equilibration under amphibolite-facies conditions.

The bytownite (An88-89) in mafic Sample 14.2 is typical of plagioclase crystallised from mafic magma and is interpreted as relict igneous plagioclase. The albite and clinozoisite in the same sample are compatible with breakdown of this calcic plagioclase during retrogression from amphibolite-facies conditions, as pargasite in the same sample indicates the rock reached amphibolite facies.

In Sample 16, perthitic intergrowths indicate subsolidus modification of the feldspar during cooling.

The evidence for a later retrograde overprint is particularly clear in Sample 28.1. Chloritisation of earlier minerals, together with irregular or embayed garnet margins, indicates later retrograde modification. Lundqvist (1962) also observed extensive chloritisation at Rävnäsudden, affecting biotite, anthophyllite, and cordierite, indicating that the assemblage was subsequently modified by retrograde hydration. The chlorite is therefore interpreted as evidence for retrograde reaction rather than as evidence that peak metamorphism only reached greenschist-facies conditions.

The retrograde textures provide stronger evidence for fluid involvement than the presence of hydrous peak minerals such as amphibole or mica. Chloritisation and later mineral growth along garnet fractures support fluid-assisted re-equilibration during cooling.

The petrographic and mineral-chemical evidence therefore records a polyphase metamorphic history.

5.2.1 Metamorphic grade

The combined petrographic and mineralogical evidence indicates that peak metamorphism on Östra Lagnö reached amphibolite-facies conditions. This interpretation is based on widespread metamorphic recrystallisation, assemblages (e.g. Site 28.1) containing pargasite, plagioclase, biotite, and garnet, and the absence of confirmed pyroxene. Upper amphibolite-facies conditions cannot be excluded, given the migmatite-like textures (Section 4.4) and the regional context, but are not demonstrated: muscovite and quartz remain widespread, no Al-silicate minerals were identified, and the leucosome-like domains have not been confirmed as partial melt. This is higher than Lundqvist (1962), who assigned the main metamorphism in the area to lower amphibolite- to epidote-amphibolite-facies conditions.

The widespread chlorite does not indicate a low peak grade, as some of it formed after the peak assemblage and therefore records the cooling and hydration history of the rocks instead. It does not by itself indicate peak greenschist facies. The same applies to epidote.

At the same time, granulite-facies metamorphism is not demonstrated. The possible pyroxene in Sample 16 is not confirmed, and no other pyroxene was identified.

The broad field of peak conditions compatible with these constraints is shown in Figure 27. It illustrates a range of possible conditions rather than a precise P-T estimate.

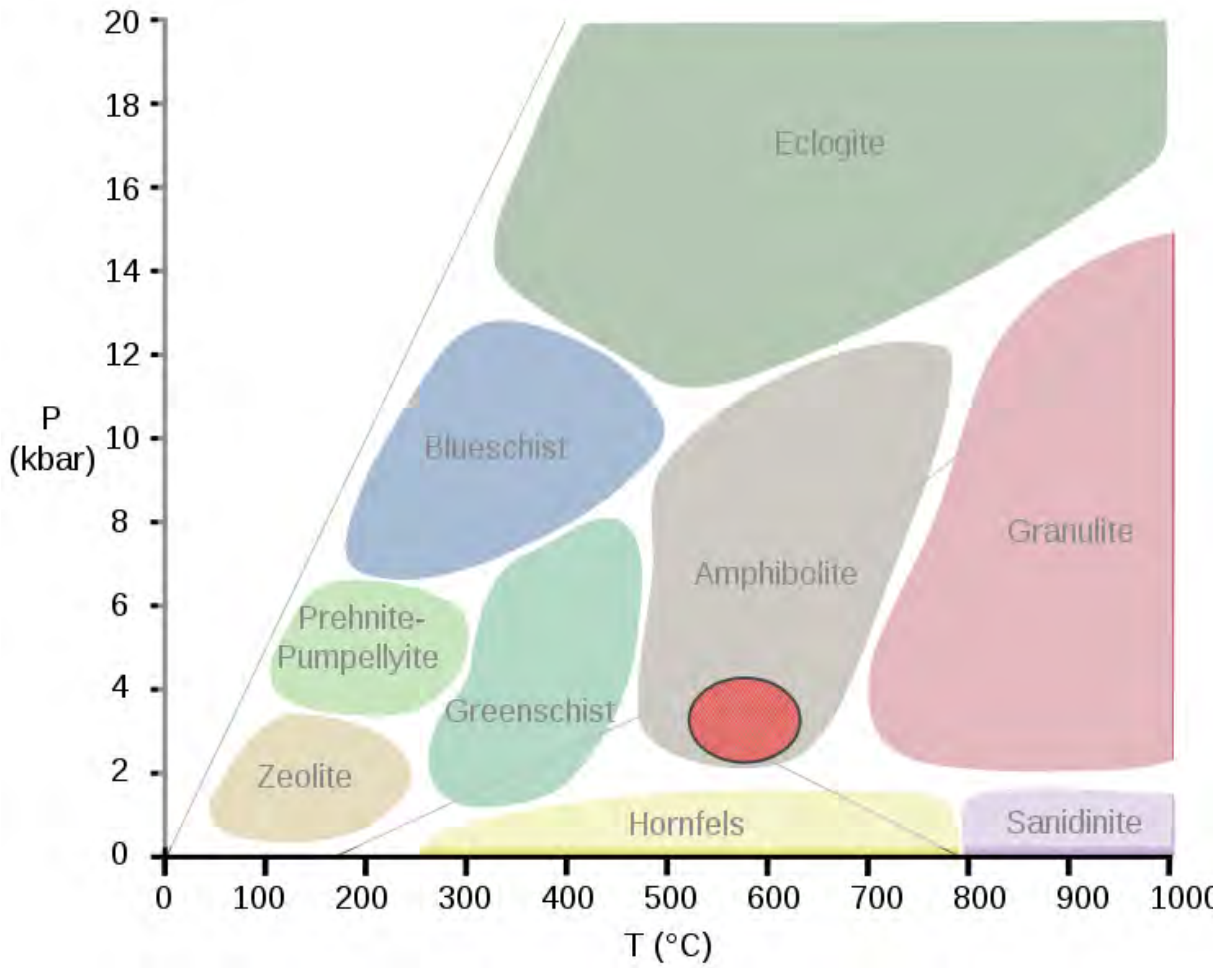


Figure 27. Metamorphic-facies diagram; the red hatched area shows the broad, qualitative field of peak metamorphic conditions on Östra Lagnö inferred from the observed mineral assemblages. Base diagram from Woudloper (2012), modified.

5.3 Regional metamorphic context

The identified peak assemblage is compatible with the low-pressure, high-temperature Buchan-type metamorphism identified within the Svecofennian province by Skelton et al. (2018).

On Utö, Talbot (2008) records sillimanite and andalusite, whereas no Al-silicate minerals were identified on Östra Lagnö, possibly reflecting lower grade or bulk-composition differences. Talbot (2008) additionally describes two stages of metamorphic mineral growth on Utö, recognised from porphyroblast core-rim relationships and deformation fabrics. The evidence from Östra Lagnö is insufficient to establish comparable separate metamorphic stages, as retrograde overprinting can occur during a single metamorphic cycle.

Stephens and Jansson (2020) and Skelton et al. (2018) describe strong spatial variation in metamorphic grade across Bergslagen, from greenschist facies to upper-amphibolite- and locally granulite-facies conditions with anatexis, with the higher grades concentrated in parts of the Stockholm archipelago. This regional variation is consistent with the relatively high-temperature assemblages observed on Östra Lagnö.

Taken together, the regional evidence supports the amphibolite- to potentially upper-amphibolite-facies interpretation developed from the Östra Lagnö mineral assemblages.

5.4 Structural evolution and deformation

Compositional layering and deformation fabrics are broadly parallel across the study area (Figure 16, Section 4.5) and indicate ductile transposition of primary layering into the regional structural grain. At less deformed

localities, layering may still reflect its original orientation, and the contrasting measurement at Site 7.2 suggests a later deformation event. Lundqvist (1962) inferred two phases of folding in the area, the younger associated with the formation of veined gneisses and affecting pegmatite dykes.

The dominant orientation is broadly consistent with previous observations from the region. Lundqvist (1962) described bedding and schistosity on the Lagnö islands as generally concordant and predominantly steeply dipping towards the NNW, while Gavelin et al. (1976) reported mainly north-easterly bedding strikes at Utö.

Folding, boudinage, and schistosity confirm that deformation was ductile and affected both the supracrustal sequence and later intrusions. Variations in schistosity intensity reflect differences in mica abundance and deformation intensity. The heterogeneous strain is linked to lithological competence as the study area is too small for significant variation in metamorphic conditions. Polyphase ductile deformation is also documented on Utö (Talbot, 2008), and regional Svecofennian successions record multiple episodes of folding capable of transposing earlier structures (Stephens and Jansson, 2020).

At a broader scale, the dominant NE-SW to ENE-WSW orientation on Östra Lagnö is compatible with the regional Svecofennian ductile deformation zones described by Wahlgren et al. (2018) (Figure 28).

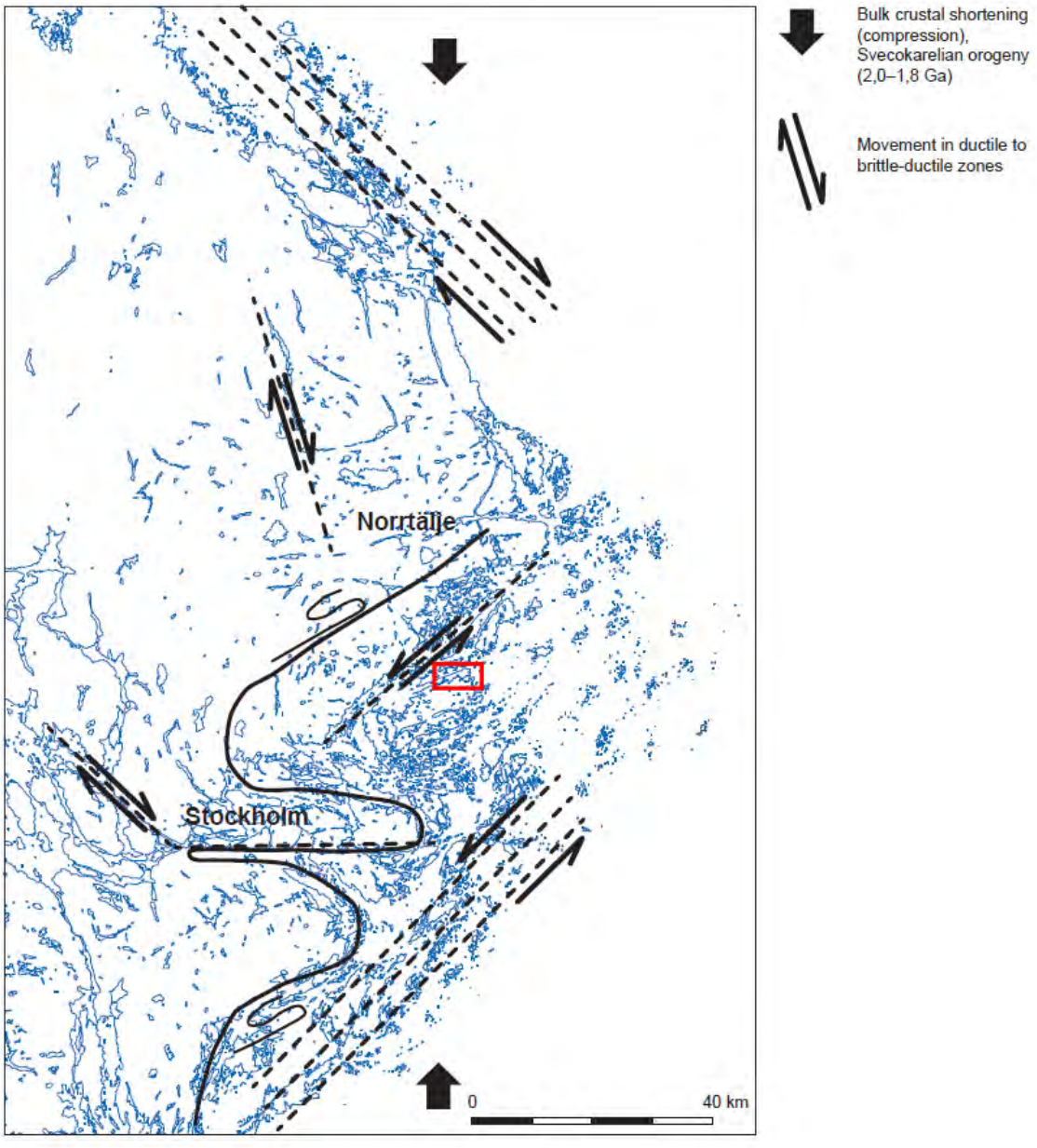


Figure 28. Regional pattern of major ductile deformation zones in eastern Sweden during the Svecokarelian

orogeny, showing the interpreted horizontal movement components and the conjugate relationship between the dextral Singö zone in north-eastern Uppland and the sinistral Örö banded series in the south-eastern Stockholm archipelago. The location of Östra Lagnö is shown in red. Modified from Wahlgren et al. (2018).

As no reliable shear-sense indicators were identified in this study, the structural evidence is compatible with the regional deformation pattern but insufficient to link the mapped structures to specific deformation zones or establish regional kinematics.

5.5 Intrusive history and relative chronology

The relative geological history of Östra Lagnö is constrained by cross-cutting and deformation relationships among several generations of intrusive rocks.

The mafic bodies within the supracrustal succession are interpreted as intrusive sheets, consistent with Lundqvist's (1962) description of generally concordant amphibolite dykes in the area. Relict bytownite in Sample 14.2 supports a mafic igneous protolith. Felsic volcanism and mafic plutonic emplacement were broadly contemporaneous in northern Bergslagen at approximately 1.89 Ga (Andersson et al., 2006), providing a regional context for their association on Östra Lagnö.

Migmatite-like textures and pale felsic material at several localities are consistent with local partial melting, as documented in higher-grade parts of the Bergslagen unit (Stephens and Jansson, 2020) and on Utö (Talbot, 2008). However, whole rock geochemistry is needed to confirm their origin. In several exposures, coarse felsic material cuts darker host rock but is itself folded, indicating emplacement or mobilisation before ductile deformation.

The contact at Sites 30-31 is consistent with intrusion of the granitoid into the felsic volcanic succession, and pegmatite intruding granite between Sites 29 and 32 establishes that the granitoid predates at least some pegmatite emplacement. The granitoid is interpreted as an early-orogenic intrusion comparable to the ∼1.91-1.87 Ga GDG association (Stephens and Jansson, 2020). Cross-cutting pegmatite dykes indicate repeated intrusion, and their occurrence in both weakly and strongly deformed parts of the succession suggests emplacement overlapped with deformation, consistent with Talbot's (2008) description of pegmatite emplacement before, during, and after ductile deformation on Utö.

The relative sequence is: formation of the felsic supracrustal succession and broadly contemporaneous early-orogenic granitoid → emplacement of earlier intrusive rocks and/or mobilisation of felsic material → deformation affecting earlier felsic and pegmatitic bodies and the granitoid → later pegmatite emplacement in multiple episodes (late-orogenic).

6 CONCLUSION: THE GEOLOGICAL EVOLUTION OF ÖSTRA LAGNÖ

The geological history of Östra Lagnö records the development of a felsic volcanic and volcaniclastic succession that was subsequently reworked, deformed, metamorphosed, and intruded. Metamorphism, deformation, partial melting and intrusive activity overlapped rather than forming a simple succession of defined events.

The felsic supracrustal succession records substantial explosive volcanism and volcaniclastic deposition, preserved as ignimbrite, ash-rich and compositionally layered units with lapilli, fiamme, and abundant plagioclase interpreted as relict pheno- or xenocrysts. This is compatible with the widespread Palaeoproterozoic felsic volcanic activity within the Bergslagen lithotectonic unit (Stephens and Jansson, 2020).

Volcanism was accompanied by sedimentary reworking. Sand- and quartz-rich intervals, coarse fragment-rich deposits, and the conglomeratic units preserve evidence of erosion, transport, and redeposition of previously formed material, while the carbonate- and skarn-bearing rocks represent an interval of carbonate sedimentation. Finely-laminated layers and grading record subaqueous deposition.

The supracrustal succession subsequently underwent substantial metamorphic and structural modification. Foliation, folding, and boudinage record polyphase deformation, mineral assemblages indicate amphibolite-facies conditions, and post-foliation mineral growth indicates that metamorphism and deformation overlapped.

Migmatite-like textures and folded pale felsic material suggest local partial melting, consistent with

migmatisation documented elsewhere in the Bergslagen domain (Stephens and Jansson, 2020).

Intrusive activity overlapped the later tectonothermal evolution. Mafic sheets were emplaced broadly contemporaneously with the felsic supracrustal succession. Granite predates at least one pegmatite generation, and pegmatite emplacement occurred in multiple stages overlapping with deformation.

At the same time, cooling was accompanied by retrograde mineral re-equilibration and locally fluid-assisted alteration. Chloritisation of mica, alteration of garnet and feldspar, chlorite associated with fractures in earlier minerals, as well as the occurrence of epidote in many samples, record modification of higher-temperature peak assemblages during retrogression.

In summary, the geological evolution of Östra Lagnö is: Felsic volcanism and volcaniclastic deposition, with broadly contemporaneous early-orogenic granitoid emplacement → local sedimentary reworking, coarse mass-flow/conglomeratic deposition, and carbonate sedimentation → burial, ductile deformation, and amphibolite-facies metamorphism → local high-temperature partial melting and melt mobilisation overlapping with continued deformation → multi-stage late-orogenic intrusive activity, including pegmatite emplacement → cooling and fluid-assisted retrograde alteration → later brittle modification, uplift, erosion, and Quaternary glacial modification.

This evolution is consistent with the regional Svecofennian framework described in the literature.

6.1 Limitations and further research

This study is limited by the absence of whole-rock geochemistry, a small number of thin sections, and EDS-only mineral chemistry without core-to-rim traverses. In the field, vegetation cover and housing development at Site 39 restricted access, preventing younging determination at several localities.

The identity and origin of the ovoid nodules and the radial amphibole at Sites 28-28.2 remain uncertain. Further petrographic work, quantitative mineral chemistry, and whole-rock geochemistry are needed to test whether these represent metamorphosed hydrothermal alteration and clarify the relationship between the different amphibole-bearing rocks.

The skarn and carbonate-bearing rocks, particularly those around Site 6, would also benefit from more detailed investigation. Mineral-chemical analysis and systematic sampling could better constrain the protolith and the reactions responsible for the calc-silicate assemblage.

Whether any of the quartz-rich units represent primary sedimentary deposits rather than recrystallised volcaniclastic material remains unresolved and would require additional sampling, including identification of preserved sedimentary textures or detrital components.

Further garnet core-to-rim analyses could test for zoning, distinguish growth stages, and constrain whether the host rock and pegmatite garnets record distinct processes.

Finally, garnet-biotite thermometry and thermodynamic modelling (Thermo-Calc) could provide quantitative P-T constraints to test the qualitative metamorphic-facies interpretation and evaluate whether upper-amphibolite-facies conditions and local partial melting are thermodynamically plausible.

7 REFERENCES

Allen, R.L., Lundström, I., Ripa, M., Simeonov, A. and Christofferson, H. (1996) 'Facies analysis of a 1.9 Ga continental margin, back-arc, felsic caldera province with diverse Zn-Pb-Ag-(Cu-Au) sulfide and Fe oxide deposits, Bergslagen region, Sweden', *Economic Geology*, 91, pp. 979-1008.

Andersson, U.B., Högdahl, K., Sjöström, H. and Bergman, S. (2006) 'Multistage growth and reworking of the Palaeoproterozoic crust in the Bergslagen area, southern Sweden: evidence from U-Pb geochronology', *Geological Magazine*, 143(5), pp. 679-697. doi: **10.1017/S0016756806002494**.

Gavelin, S., Lundström, I. and Norström, S. (1976) *Svecofennian stratigraphy on Utö, Stockholm archipelago: Correlations with Finland and Sweden*. Sveriges geologiska undersökning, Series C, No. 719. Stockholm: Sveriges geologiska undersökning, 44 pp.

Hawthorne, F.C., Oberti, R., Harlow, G.E., Maresch, W.V., Martin, R.F., Schumacher, J.C. and Welch, M.D. (2012) 'Nomenclature of the amphibole supergroup', *American Mineralogist*, 97, 2031-2048.

Hernández-Filiberto, L., Roda-Robles, E., Simmons, W.B. and Webber, K.L. (2021) 'Garnet as Indicator of Pegmatite Evolution: The Case Study of Pegmatites from the Oxford Pegmatite Field (Maine, USA)', Minerals, 11(8), 802. doi: 10.3390/min11080802.

Lundqvist, T. (1962) *Det svekofenniska suprakrustalstråket mellan Ljusterö och Rödlöga i Stockholms norra skärgård*. Sveriges geologiska undersökning, Series C, No. 585. Stockholm: Sveriges geologiska undersökning. (In Swedish. Translated throughout this text.)

Skelton, A., Mansfeld, J., Ahlin, S., Lundqvist, T., Linde, J. and Nilsson, J. (2018) 'A compilation of metamorphic pressure-temperature estimates from the Svecofennian province of eastern and central Sweden', *GFF*, 140(1), pp. 1-10. doi: 10.1080/11035897.2017.1414074.

Stephens, M.B. and Jansson, N.F. (2020) 'Paleoproterozoic (1.9-1.8 Ga) syn-orogenic magmatism, sedimentation and mineralization in the Bergslagen lithotectonic unit, Svecofennian orogen', in Stephens, M.B. and Bergman Weihed, J. (eds.) *Sweden: Lithotectonic Framework, Tectonic Evolution and Mineral Resources*. Geological Society, London, Memoirs, 50, pp. 155-206. doi: 10.1144/M50-2017-40.

Talbot, C.J. (2008) 'Palaeoproterozoic crustal building in NE Utö, southern Svecofennides, Sweden', *GFF*, 130(2), pp. 49-70.

Wahlgren, C.-H., Schoning, K., Tenne, M. and Hansen, L.M. (2018) *The geological evolution of Stockholm - bedrock, Quaternary deposits and experience from infrastructure projects*. SGU-rapport 2018:08. Uppsala: Sveriges geologiska undersökning.

Woudloper (2012) *Metamorphic Facies Diagram.png*, retouched by Jantho6 [image]. Wikimedia Commons. Available at: https://commons.wikimedia.org/wiki/File:Metamorphic_Facies_Diagram.png (Accessed: 30 September 2026).

AI was used during the preparation of this thesis to assist with language editing and proofreading of the text, and to help write a Python script used to generate the ternary diagrams presented in this work. All scientific content, data, analysis, photos, and interpretation are the author's own.

8 APPENDIX

Table F

Table F. The field characteristics of the felsic volcanic or volcaniclastic rocks. The selected field sites are representative of the main lithological and textural characteristics observed across the mapped area. - = not recorded.

Site	Field character / lithology	Primary textures	Deformation / other observations
1	Distinctly layered, fine-grained felsic rock with parallel mafic material	mm-scale parallel layers; possible ash layers	Local folding and migmatisation; bedding vs. deformation-stretched layering uncertain
5	Layered to massive, homogeneous felsic rock; possible ignimbrite (recrystallised ash, abundant quartz)	Possible lapilli; fiamme; possible quartz fragments	Ash textures better preserved than in surrounding migmatites
6	Layered succession of fine ash and sand layers	Ash layers <1mm; two sand layers (∼40cm wide, ∼5 m long) with dark mineral-rich bands at their bases	Lateral deformation
7	Alternating clay- and sand-rich layers	Possible graded bedding; possible younging to the N (7.1, 7.3)	Competency contrasts between layers
8	Layered felsic rock	Possible wall-rock and volcanic fragments; possible agglomerate or mass-flow deposit	-
12	Layered to massive, homogeneous felsic rock; possible ignimbrite	Fine-grainedmm-scale layers with possible fining northward; lapilli (recorded or suspected); possible fiamme	Primary vs. deformation origin of layering uncertain
15	Massive felsic rock; possible ignimbrite	Lapilli ∼1-2cm (largest recorded)	-
16	Layered to massive felsic rock; possible ignimbrite with sand-sized, quartz-rich grains	Lapilli recorded nearby (sample 16); possible fragments	Fragments vs. deformed layers unresolved
19	Layered to massive felsic rock; possible ignimbrite	Lapilli up to ∼7mm	Schistose material present
21	Massive felsic rock; possible ignimbrite	Lapilli confidently identified; none observed at 21.1 (pegmatite)	Moderate deformation
22	Massive felsic rock	Lapilli; larger clasts up to ∼10cm; possible fiamme (at least one)	Many lapilli stretched/aligned
26	Large, homogeneous outcrop; probable ignimbrite; finer	Lapilli definitely present; other fragments; possible fiamme	Little visible deformation

Site	Field character / lithology	Primary textures	Deformation / other observations
	layering on SE side (060/60 NW)	(also 26.2)	
28	Layered; greenish schistose rock (possible greenschist)	Possible lapilli (28, 28.1, 28.2); possible fragments/xenoliths (28.2)	Garnet-rich host rock
34	Layered felsic rock	Numerous possible lapilli and fragments, up to ~10 × 3cm	Schistosity, boudinage and folds; possible migmatisation; key site for separating volcanic clasts from deformation structures
36	Massive felsic rock	Abundant fiamme (most abundant at this site), ~20cm long and 5-7cm wide	Fiamme visibly deformed
37	Layered	Possible fiamme (37.1)	Fiamme strongly stretched (37.1)

Table EMP

Table EMP. Petrographic and SEM-EDS data of felsic volcanic rocks. All reported mineral phases are listed for Sample 50; grain size, textures, fabric, and modal proportions were not assessed.

Sample	Mineralogy and provisional visual proportions	Grain size and texture	Fabric and alteration
1.1	Quartz, plagioclase and unidentified feldspar, and muscovite.	Moderately to coarsely grained, locally granoblastic, with finer-grained intervals between coarser domains.	Alternating muscovite-rich and mica-poor layers; muscovite locally preferentially aligned.
8	Quartz ~40%, plagioclase ~35%, muscovite ~20% and biotite ~5%.	Locally granoblastic; rounded quartz-feldspar-rich domains locally coarser than the surrounding matrix (Figure 7); locally larger plagioclase grains.	Consistent mica alignment not documented.
11	Quartz, plagioclase, and muscovite.	Strongly variable grain size, with large quartz and muscovite grains and a finer-grained matrix; locally granoblastic; locally rounded quartz-feldspar-rich domains.	Large mica flakes; consistent mica alignment not documented.
13.1	Quartz, plagioclase and unidentified feldspar, muscovite, and biotite; combined mica ~40%, with the remaining phases not separately quantified.	Predominantly granoblastic quartz-feldspar assemblage; variable grain size; rounded quartz-feldspar-rich domains locally present.	Muscovite and biotite preferentially aligned and concentrated into layers, schistose in hand sample.
16	Quartz:feldspar:muscovite approximately 45:45:10, (normalised excl. minor and	Moderately to coarsely grained and texturally	No mica alignment recorded.

	accessory). Feldspar: plagioclase and K-feldspar; some K-feldspar is perthitic, while local possible tartan twinning may indicate microcline. Minor amphibole, epidote, and chlorite.	variable; locally granoblastic; lamellar perthitic intergrowths present.	
20	Quartz, plagioclase and other feldspars, and muscovite occur in approximately equal proportions	Granoblastic quartz-feldspar domains with aligned mica-rich bands.	Biotite and muscovite preferentially aligned and concentrated in mica-rich layers; possible compositional layering.
28.1	Quartz, garnet, plagioclase ~15%, muscovite ~15%, biotite, abundant chlorite, and minor amphibole and epidote.	Generally finer grained than 35.1, although large quartz and plagioclase grains occur; garnet heavily included, fractured and locally rounded.	Chloritic alteration; mica foliation around garnet; abundant chlorite and chloritised mica; chlorite occurs within garnet fractures; micas preferentially aligned; garnet overgrows mica fabric
35.1	Quartz and feldspar (plagioclase and K-feldspar) dominate, with abundant biotite and subordinate garnet. Garnet is visually estimated at approximately 5-10%. Plagioclase includes andesine (confirmed by SEM-EDS, An33-35).	Alternating coarser-grained domains and a finer-grained granoblastic layer; garnet locally fractured.	Biotite-defined fabric overgrown by post-deformation garnet; chlorite occurs within garnet fractures; possible local replacement of garnet at irregular margins; compositional layering of uncertain origin.
50	Phases identified by SEM-EDS: chlorite, albite-rich plagioclase, quartz, K-rich white mica, epidote, F-bearing titanite, rutile, ilmenite, Mn-bearing ilmenite, and opaque phases. Possible apatite or fluorapatite.	Not assessed.	Not assessed.

Table M

Table M. Field occurrences and characteristics of mafic rocks.

Site(s)	Occurrence and measurements	Uncertainty and Notes
9	Two parallel, planar mafic bands with sharp contacts within ignimbrite-like felsic volcanic rock, continuing below sea level.	Clearest intrusive geometry; occur within the upper unit of the logged section (Figure 13).
14	Two parallel mafic bands, approximately 7 and 10cm wide.	Possibly intrusive; relationship to host-rock layering not recorded.
17.2	Mafic band approximately 20-30cm wide, 079/18° N.	Possibly intrusive.
22	Tabular mafic body	Possibly intrusive.

35	Tabular mafic material.	Possibly intrusive.
13	Approximately 7 m wide schistose mafic units occur within an alternating mafic-felsic succession.	Possibly intrusive mafic bodies or compositional layering within the metamorphosed succession.
19, 20, and 28	Felsic sites with mafic material.	No direct correlation between mafic field material and petrographic samples 20 and 28

Tables SM: Structural Orientation Measurements

Strike orientations were used to construct the layering and foliation/deformation-fabric rose diagrams (Figure 16). Dip and dip direction are retained here as part of the complete planar measurements.

Table SM-A. Layering measurements used in the layering rose diagram (n = 16). Site 16 (081/79° N) is excluded here and included in the deformation-fabric table instead.

Site	Strike (°)	Dip (°)	Dip direction	Structural type	Field notes
1	67	80	N	Layering	Linear layers; uncertain whether primary bedding or deformation-stretched layering.
2	66	84	N	Layering	Similar layered rock package to Site 1; possible sandy/ash layer.
5	59	70	N	Layering	Measurement at recrystallised ash / ignimbrite locality; not explicitly measured on fiamme or lapilli.
6	68	81	N	Layering	Fine ash layers with two thicker sand-rich layers.
8	64	78	N	Layering	Felsic volcanic/rhyolite; possible subvolcanic or volcaniclastic/mass-flow unit.
12	71	82	N	Layering	Fine-grainedmm-scale layers; primary depositional layering versus deformation-generated banding uncertain.
16	81	17	N	Layering	First measurement at Site 16; possible fragments/deformed layers in quartz-rich sand-sized rock.
17	71	69	N	Layering	Felsic volcanic in contact with schistose

					rock and intruded by pegmatite.
18	69	60	N	Layering	Ignimbrite with possible lapilli and schistose bands.
19	66	62	N	Layering	Ignimbrite with lapilli up to ~7mm; schistose material present.
20	67	62	N	Layering	Fine- and sand-sized domains with schistose bands; pegmatite and mafic sections also present.
23	91	16	N	Layering	Main orientation of layered/felsic volcanic rock
26	60	60	NW	Layering	Layers reappear on southeast side of otherwise homogeneous probable ignimbrite.
33	70	60	N	Layering	Felsic volcanic with possible tiny fragments/lapilli; confidence in fragments low.
35	60	71	N	Layering	Lundqvist-style 'felsic volcanic with mica'; possible volcanic fragments/lapilli.
37	73	60	N	Layering	Felsic volcanic with large pegmatite intrusions; very little deformation.

Table SM-B. Foliation and deformation-fabric measurements used in the fabric rose diagram (n = 8).

Site	Strike (°)	Dip (°)	Dip direction	Structural type	Field notes
7	70	71	N	Foliation / deformation fabric	Measured on foliation. Included because it is a recorded strike/dip measurement, although schistosity extent is mapped as polygon hatch.
7.2	40	84	S	Foliation / deformation	

				fabric	
13	76	81	N	Foliation / deformation fabric	Schistose mafic rock with alternating mafic-felsic succession; measurement may represent fabric/layering.
16	81	79	N	Foliation / deformation fabric	Orientation taken from lapilli-bearing part of Site 16; treated as lapilli/deformation fabric rather than layering.
17.1	72	67	N	Foliation / deformation fabric	Two schistose bands with felsic volcanic between and around them.
22	145	15	N	Foliation / deformation fabric	Taken from clasts. No clear bedding visible.
35.1	60	48	N	Foliation / deformation fabric	No clear layering; measurement taken from orientation of schistose fabric.
36	75	60	N	Foliation / deformation fabric	Orientation measured directly on fiamme.

Table SM-C. Other field orientation measurements excluded from the rose diagrams (n = 4). Retained as field observations but excluded because they do not represent confidently identified in-situ layering or deformation fabric.

Site	Strike/trend (°)	Dip/plunge (°)	Direction	Feature / lithology	Field notes and reason for exclusion
17.2	79	18	N	Mafic feature	Orientation recorded from mafic band; its relationship to layering was not established.
23	176	50	W	Orientation of rotated block	outlying orientation from a rotated block; probably glacial striations
29	148	39	W	Surface striations (possibly	Glacial striations

				glacial)	
35	65	15	N	Mafic feature	Orientation recorded from mafic material; its relationship to layering or deformation fabric was not established.

SEM-EDS Composition Tables

The following tables report full point-by-point SEM-EDS compositions for garnet, amphibole, and feldspar (plagioclase and alkali feldspar), calculated on the oxygen basis stated for each mineral (garnet: 12 O; amphibole: 23 O; feldspar: 8 O). Analytical totals deviate from 100% (c. 79-108 wt%), reflecting surface irregularities, beam overlap with adjacent phases and, for hydrous phases, unanalysed H_2O. As mineral formulae were calculated on a fixed oxygen basis, classification is based on cation ratios, and stoichiometry (cation sum and Si-Al proportions) was used as the main quality criterion. Analyses with non-stoichiometric compositions or containing elements foreign to the mineral (e.g. Mg and Fe in feldspar) were excluded from the ternary diagrams; analyses with totals outside c. 95-103 wt% but acceptable stoichiometry are retained and should be interpreted with caution.

Each mineral is reported as atomic % (the basis for all calculations in this thesis), oxide wt%, and cation proportions per formula unit (Tables A1c, A2e, A3c and A4c). Cations were calculated as atomic%(element) ÷ atomic%(O) × N, where N is the oxygen basis.

Garnet

Table A1a. SEM-EDS garnet compositions (atomic %, 12-oxygen basis).

Sample, point	Mg	Al	Si	Ca	Mn	Fe	O	Total wt%	Cation sum (12 O)
28.1, pt. 42	1.89	9.96	14.71	1.37	1.23	10.98	59.85	105.34	8.05
28.1, pt. 1	1.91	10.00	14.70	1.25	1.10	11.19	59.85	102.83	8.05
28.1, pt. 13	1.89	9.80	14.79	1.40	1.04	11.23	59.85	106.28	8.05
28.1, pt. 14	1.93	10.07	14.75	1.09	1.05	11.23	59.89	83.12	8.04
20.1, pt. 3	-	10.01	14.63	0.06	8.70	6.78	59.82	99.30	8.06
20.1, pt. 4	-	9.92	14.66	0.08	8.77	6.76	59.81	98.82	8.06
20.1, pt. 5	0.27	10.03	14.51	0.06	8.30	7.06	59.76	104.49	8.08
20.1, pt. 6	0.28	9.92	14.61	0.07	8.16	7.18	59.78	99.56	8.07
20.1, pt. 10	0.30	9.87	14.75	0.18	8.00	7.05	59.84	104.00	8.05
35.1, pt. 12	1.26	10.07	14.67	0.57	0.52	13.07	59.85	100.02	8.05
35.1, pt. 27	1.36	10.04	14.61	0.58	0.62	12.97	59.82	105.12	8.06
35.1, pt. 33	1.26	10.04	14.74	0.58	0.86	12.64	59.88	100.00	8.04
35.1, pt. 50	1.38	9.99	14.76	0.53	0.51	12.95	59.88	105.81	8.04

Table A1b. SEM-EDS garnet compositions (wt% oxide, 12-oxygen basis).

Sample, point	MgO	Al2O3	SiO2	CaO	MnO	FeO	Total	Cation sum (12 O)
28.1, pt. 42	3.32	22.09	38.46	3.35	3.78	34.33	105.34	8.05
28.1, pt. 1	3.27	21.65	37.49	2.98	3.32	34.13	102.83	8.05
28.1, pt. 13	3.35	21.91	38.97	3.45	3.22	35.37	106.28	8.05
28.1, pt. 14	2.67	17.64	30.45	2.09	2.55	27.72	83.12	8.04
20.1, pt. 3	-	20.29	34.97	0.13	24.54	19.37	99.30	8.06
20.1, pt. 4	-	19.99	34.83	0.18	24.60	19.21	98.82	8.06
20.1, pt. 5	0.46	21.43	36.53	0.13	24.68	21.25	104.49	8.08
20.1, pt. 6	0.44	20.19	35.05	0.15	23.12	20.61	99.56	8.07
20.1, pt. 10	0.50	21.05	37.08	0.41	23.75	21.20	104.00	8.05
35.1, pt. 12	2.07	20.94	35.93	1.29	1.51	38.28	100.02	8.05
35.1, pt. 27	2.34	21.94	37.62	1.41	1.89	39.92	105.12	8.06
35.1, pt. 33	2.08	20.89	36.16	1.32	2.50	37.06	100.00	8.04
35.1, pt. 50	2.40	22.01	38.32	1.29	1.57	40.22	105.81	8.04

Table A1c. SEM-EDS garnet cation proportions per formula unit (12-oxygen basis).

Sample, point	Mg	Al	Si	Ca	Mn	Fe	Cation sum (12 O)
28.1, pt. 42	0.379	1.997	2.949	0.275	0.247	2.202	8.05
28.1, pt. 1	0.383	2.005	2.947	0.251	0.221	2.244	8.05
28.1, pt. 13	0.379	1.965	2.965	0.281	0.209	2.252	8.05
28.1, pt. 14	0.387	2.018	2.955	0.218	0.210	2.250	8.04
20.1, pt. 3	-	2.008	2.935	0.012	1.745	1.360	8.06
20.1, pt. 4	-	1.990	2.941	0.016	1.760	1.356	8.06
20.1, pt. 5	0.054	2.014	2.914	0.012	1.667	1.418	8.08
20.1, pt. 6	0.056	1.991	2.933	0.014	1.638	1.441	8.07
20.1, pt. 10	0.060	1.979	2.958	0.036	1.604	1.414	8.05
35.1, pt. 12	0.253	2.019	2.941	0.114	0.104	2.621	8.05
35.1, pt. 27	0.273	2.014	2.931	0.116	0.124	2.602	8.06
35.1, pt. 33	0.253	2.012	2.954	0.116	0.172	2.533	8.04
35.1, pt. 50	0.277	2.002	2.958	0.106	0.102	2.595	8.04

Amphibole

Ternary diagram positions were calculated from atomic %; oxide wt% is included here for reference.

Table A2a. SEM-EDS amphibole compositions (atomic %, 23-oxygen basis), Sample 14.2 calculation input. Point 23 is a compositional/stoichiometric outlier (see Section 4.7.2).

Sample, point	Na	Mg	Al	Si	K	Ca	Ti	Mn	Fe	O	Total wt%	Cation sum (23 O)	Included?
14.2, pt. 7	0.71	4.44	5.73	16.52	0.53	5.12	0.20	0.19	7.07	59.48	98.46	15.66	Yes
14.2, pt. 20	0.79	4.66	5.55	16.54	0.60	5.11	0.25	0.21	6.85	59.43	97.57	15.70	Yes
14.2, pt. 23	2.63	6.57	8.01	12.86	0.10	6.45	-	0.07	5.56	57.75	92.95	16.83	No
14.2, pt. 29	0.82	4.70	5.64	16.51	0.59	5.06	0.23	0.20	6.82	59.43	88.30	15.70	Yes
14.2, pt. 37	0.84	4.37	5.87	16.34	0.56	5.12	0.18	0.22	7.12	59.38	93.53	15.73	Yes
14.2, pt. 38	0.73	4.77	5.62	16.49	0.63	5.00	0.22	0.20	6.93	59.42	88.19	15.71	Yes

Table A2b. SEM-EDS amphibole compositions (wt% oxide, 23-oxygen basis), Sample 14.2. Point 23 is a compositional/stoichiometric outlier (see Section 4.9.2, 5.3.2).

Sample, point	Na2O	MgO	Al2O3	SiO2	K2O	CaO	TiO2	MnO	FeO	Total	Cation sum (23 O)	Included?
14.2, pt. 7	0.93	7.54	12.32	41.85	1.05	12.10	0.68	0.58	21.40	98.46	15.66	Yes
14.2, pt. 20	1.02	7.87	11.85	41.58	1.18	12.00	0.82	0.63	20.61	97.57	15.70	Yes
14.2, pt. 23	3.30	10.72	16.51	31.26	0.18	14.63	-	0.21	16.15	92.95	16.83	No
14.2, pt. 29	0.96	7.18	10.91	37.61	1.05	10.75	0.70	0.54	18.59	88.30	15.70	Yes
14.2, pt. 37	1.04	7.05	11.97	39.27	1.05	11.50	0.58	0.61	20.47	93.53	15.73	Yes
14.2, pt. 38	0.85	7.28	10.84	37.47	1.12	10.60	0.66	0.55	18.82	88.19	15.71	Yes

Table A2c. SEM-EDS amphibole compositions (atomic %, 23-oxygen basis), Sample 28.1, calculation input. Point 21 also contains 0.07 atomic % Cr (not shown), included in Total and Cation sum.

Sample, point	Na	Mg	Al	Si	K	Ca	Ti	Mn	Fe	O	Total wt%	Cation sum (23 O)	Included?
28.1, pt. 9	1.43	5.81	6.89	15.60	0.12	3.96	0.09	0.13	6.78	59.18	93.36	15.86	Yes
28.1, pt. 12	-	8.51	1.10	20.32	-	0.33	-	0.23	9.09	60.43	100.56	15.06	Yes
28.1, pt. 17	-	8.55	1.01	20.36	-	0.25	-	0.21	9.19	60.43	79.41	15.06	Yes
28.1, pt. 21	1.77	4.68	7.15	15.99	0.10	4.18	0.11	0.13	6.43	59.39	98.19	15.73	Yes

Table A2d. SEM-EDS amphibole compositions (wt% oxide, 23-oxygen basis), Sample 28.1. Point 21 also contains 0.23 wt% Cr2O3 (not shown), included in Total and Cation sum.

Sample, point	Na2O	MgO	Al2O3	SiO2	K2O	CaO	TiO2	MnO	FeO	Total	Cation sum (23 O)	Included?
28.1, pt. 9	1.79	9.52	14.26	38.07	0.23	9.03	0.31	0.37	19.79	93.36	15.86	Yes

Sample, point	Na2O	MgO	Al2O3	SiO2	K2O	CaO	TiO2	MnO	FeO	Total	Cation sum (23 O)	Included?
28.1, pt. 12	-	14.94	2.44	53.20	-	0.81	-	0.71	28.46	100.56	15.06	Yes
28.1, pt. 17	-	11.85	1.78	42.07	-	0.47	-	0.52	22.72	79.41	15.06	Yes
28.1, pt. 21	2.35	8.07	15.61	41.14	0.21	10.04	0.37	0.41	19.77	98.19	15.73	Yes

Table A2e. SEM-EDS amphibole cation proportions per formula unit (23-oxygen basis), Samples 14.2 and 28.1. Cation sum for pt. 21 includes 0.03 Cr (not shown).

Sample, point	Na	Mg	Al	Si	K	Ca	Ti	Mn	Fe	Cation sum (23 O)	Included?
14.2, pt. 7	0.275	1.717	2.216	6.388	0.205	1.980	0.077	0.073	2.734	15.66	Yes
14.2, pt. 20	0.306	1.803	2.148	6.401	0.232	1.978	0.097	0.081	2.651	15.70	Yes
14.2, pt. 23	1.047	2.617	3.190	5.122	0.040	2.569	-	0.028	2.214	16.83	No
14.2, pt. 29	0.317	1.819	2.183	6.390	0.228	1.958	0.089	0.077	2.639	15.70	Yes
14.2, pt. 37	0.325	1.693	2.274	6.329	0.217	1.983	0.070	0.085	2.758	15.73	Yes
14.2, pt. 38	0.283	1.846	2.175	6.383	0.244	1.935	0.085	0.077	2.682	15.71	Yes
28.1, pt. 9	0.556	2.258	2.678	6.063	0.047	1.539	0.035	0.051	2.635	15.86	Yes
28.1, pt. 12	-	3.239	0.419	7.734	-	0.126	-	0.088	3.460	15.06	Yes
28.1, pt. 17	-	3.254	0.384	7.749	-	0.095	-	0.080	3.498	15.06	Yes
28.1, pt. 21	0.685	1.812	2.769	6.192	0.039	1.619	0.043	0.050	2.490	15.73	Yes

Plagioclase

Table A3a. SEM-EDS plagioclase compositions (atomic %, 8-oxygen basis) - calculation input. Analyses marked "No" (non-stoichiometric or containing Mg and Fe) are excluded from the ternary diagram (Figure 26).

Sample, point	Na	Mg	Al	Si	K	Ca	Fe	O	Total wt%	Cation sum (8 O)	Included?
14.2, pt. 15	7.30	-	9.53	21.70	-	-	0.07	61.41	79.45	5.03	Yes
14.2, pt. 16	6.77	-	8.68	22.71	-	-	-	61.83	80.57	4.94	Yes
14.2, pt. 24	0.88	-	14.55	15.97	-	7.06	0.14	61.40	83.35	5.03	Yes
14.2, pt. 33	0.94	-	14.59	16.10	-	6.90	-	61.47	89.66	5.01	Yes
28.1, pt. 48	3.90	-	11.29	19.81	0.55	2.83	-	61.61	98.43	4.98	Yes
28.1, pt. 2	3.81	-	11.54	19.27	-	3.81	-	61.57	98.04	4.99	Yes
35.1, pt. 19	4.95	-	10.38	20.44	-	2.65	-	61.58	99.94	4.99	Yes
35.1, pt. 32	5.01	-	10.32	20.50	-	2.54	0.06	61.58	103.27	4.99	Yes
35.1, pt. 44	4.99	-	10.29	20.57	-	2.54	-	61.61	97.52	4.98	Yes

Sample, point	Na	Mg	Al	Si	K	Ca	Fe	O	Total wt%	Cation sum (8 O)	Included?
35.1, pt. 48	4.99	-	10.39	20.47	-	2.57	-	61.59	92.32	4.99	Yes
50, pt. 8	6.65	-	8.30	22.69	0.25	0.33	0.10	61.70	86.84	4.97	Yes
50, pt. 14	5.46	0.37	9.15	21.79	0.89	0.32	0.42	61.59	100.09	4.99	No
50, pt. 15	5.92	0.55	9.14	21.56	0.48	0.55	0.34	61.46	108.41	5.02	No
50, pt. 23	6.86	-	8.18	22.93	0.14	0.13	-	61.76	79.93	4.95	Yes

Table A3b. SEM-EDS plagioclase compositions (wt% oxide, 8-oxygen basis).

Sample, point	Na2O	MgO	Al2O3	SiO2	K2O	CaO	FeO	Total	Cation sum (8 O)	Included?
14.2, pt. 15	8.89	-	19.10	51.26	-	-	0.19	79.45	5.03	Yes
14.2, pt. 16	8.38	-	17.68	54.50	-	-	-	80.57	4.94	Yes
14.2, pt. 24	1.07	-	28.97	37.47	-	15.46	0.38	83.35	5.03	Yes
14.2, pt. 33	1.22	-	31.35	40.77	-	16.31	-	89.66	5.01	Yes
28.1, pt. 48	5.75	-	27.34	56.56	1.24	7.54	-	98.43	4.98	Yes
28.1, pt. 2	5.57	-	27.76	54.62	-	10.09	-	98.04	4.99	Yes
35.1, pt. 19	7.44	-	25.67	59.61	-	7.22	-	99.94	4.99	Yes
35.1, pt. 32	7.78	-	26.38	61.75	-	7.15	0.22	103.27	4.99	Yes
35.1, pt. 44	7.33	-	24.87	58.57	-	6.75	-	97.52	4.98	Yes
35.1, pt. 48	6.93	-	23.75	55.18	-	6.46	-	92.32	4.99	Yes
50, pt. 8	8.82	-	18.11	58.34	0.50	0.78	0.29	86.84	4.97	Yes
50, pt. 14	8.27	0.73	22.78	63.92	2.04	0.89	1.47	100.09	4.99	No
50, pt. 15	9.73	1.17	24.70	68.69	1.21	1.63	1.28	108.41	5.02	No
50, pt. 23	8.40	-	16.49	54.48	0.27	0.29	-	79.93	4.95	Yes

Table A3c. SEM-EDS plagioclase cation proportions per formula unit (8-oxygen basis).

Sample, point	Na	Mg	Al	Si	K	Ca	Fe	Cation sum (8 O)	Included?
14.2, pt. 15	0.951	-	1.241	2.827	-	-	0.009	5.03	Yes
14.2, pt. 16	0.876	-	1.123	2.938	-	-	-	4.94	Yes
14.2, pt. 24	0.115	-	1.896	2.081	-	0.920	0.018	5.03	Yes
14.2, pt. 33	0.122	-	1.899	2.095	-	0.898	-	5.01	Yes
28.1, pt. 48	0.506	-	1.466	2.572	0.071	0.367	-	4.98	Yes
28.1, pt. 2	0.495	-	1.499	2.504	-	0.495	-	4.99	Yes
35.1, pt. 19	0.643	-	1.348	2.655	-	0.344	-	4.99	Yes

Sample, point	Na	Mg	Al	Si	K	Ca	Fe	Cation sum (8 O)	Included?
35.1, pt. 32	0.651	-	1.341	2.663	-	0.330	0.008	4.99	Yes
35.1, pt. 44	0.648	-	1.336	2.671	-	0.330	-	4.98	Yes
35.1, pt. 48	0.648	-	1.350	2.659	-	0.334	-	4.99	Yes
50, pt. 8	0.862	-	1.076	2.942	0.032	0.043	0.013	4.97	Yes
50, pt. 14	0.709	0.048	1.189	2.830	0.116	0.042	0.055	4.99	No
50, pt. 15	0.771	0.072	1.190	2.806	0.062	0.072	0.044	5.02	No
50, pt. 23	0.889	-	1.060	2.970	0.018	0.017	-	4.95	Yes

Alkali feldspar

Table A4a. SEM-EDS alkali feldspar compositions (atomic %, 8-oxygen basis) - calculation input. Analyses marked "No" (non-stoichiometric or containing Mg and Fe) are excluded from the ternary diagram (Figure 26).

Sample, point	Na	Mg	Al	Si	K	Ca	Fe	Ba	O	Total wt%	Cation sum (8 O)	Included?
14.2, pt. 14	0.26	-	7.76	22.87	7.58	-	0.10	-	61.42	101.37	5.02	Yes
14.2, pt. 19	0.15	-	7.79	22.96	7.61	-	-	-	61.49	99.52	5.01	Yes
14.2, pt. 21	0.24	0.14	10.27	21.17	6.49	-	0.20	-	61.47	101.00	5.01	No
14.2, pt. 32	0.27	-	7.78	22.93	7.51	-	-	0.05	61.46	91.15	5.02	Yes
14.2, pt. 39	1.19	1.17	8.29	21.86	5.84	-	0.42	-	61.24	91.95	5.06	No
28.1, pt. 5	0.13	-	7.83	22.84	7.69	-	0.10	-	61.42	88.79	5.03	Yes
20.1, pt. 13	0.30	-	7.79	22.92	7.55	-	-	-	61.44	95.08	5.02	Yes
20.1, pt. 17	0.37	-	7.86	22.83	7.53	-	-	-	61.40	98.06	5.03	Yes
20.1, pt. 18	0.20	-	7.84	22.88	7.63	-	-	-	61.45	102.06	5.02	Yes
20.1, pt. 22	-	-	7.74	22.91	7.74	-	0.15	-	61.45	92.61	5.02	Yes
35.1, pt. 39	0.26	-	7.79	22.97	7.19	-	0.08	0.15	61.57	96.69	4.99	Yes

Table A4b. SEM-EDS alkali feldspar compositions (wt% oxide, 8-oxygen basis).

Sample, point	Na2O	MgO	Al2O3	SiO2	K2O	CaO	FeO	BaO	Total	Cation sum (8 O)	Included?
14.2, pt. 14	0.38	-	18.72	65.02	16.89	-	0.35	-	101.37	5.02	Yes
14.2, pt. 19	0.22	-	18.46	64.17	16.68	-	-	-	99.52	5.01	Yes
14.2, pt. 21	0.35	0.28	24.84	60.33	14.50	-	0.70	-	101.00	5.01	No
14.2, pt. 32	0.36	-	16.87	58.58	15.05	-	-	0.30	91.15	5.02	Yes
14.2, pt. 39	1.59	2.04	18.28	56.83	11.91	-	1.29	-	91.95	5.06	No

Sample, point	Na2O	MgO	Al2O3	SiO2	K2O	CaO	FeO	BaO	Total	Cation sum (8 O)	Included?
28.1, pt. 5	0.16	-	16.52	56.81	14.99	-	0.31	-	88.79	5.03	Yes
20.1, pt. 13	0.42	-	17.65	61.20	15.80	-	-	-	95.08	5.02	Yes
20.1, pt. 17	0.53	-	18.37	62.89	16.27	-	-	-	98.06	5.03	Yes
20.1, pt. 18	0.29	-	19.07	65.57	17.13	-	-	-	102.06	5.02	Yes
20.1, pt. 22	-	-	17.02	59.38	15.73	-	0.48	-	92.61	5.02	Yes
35.1, pt. 39	0.36	-	17.84	62.01	15.22	-	0.25	1.01	96.69	4.99	Yes

Table A4c. SEM-EDS alkali feldspar cation proportions per formula unit (8-oxygen basis).

Sample, point	Na	Mg	Al	Si	K	Ca	Fe	Ba	Cation sum (8 O)	Included?
14.2, pt. 14	0.034	-	1.011	2.979	0.987	-	0.013	-	5.02	Yes
14.2, pt. 19	0.020	-	1.013	2.987	0.990	-	-	-	5.01	Yes
14.2, pt. 21	0.031	0.018	1.337	2.755	0.845	-	0.026	-	5.01	No
14.2, pt. 32	0.035	-	1.013	2.985	0.978	-	-	0.007	5.02	Yes
14.2, pt. 39	0.155	0.153	1.083	2.856	0.763	-	0.055	-	5.06	No
28.1, pt. 5	0.017	-	1.020	2.975	1.002	-	0.013	-	5.03	Yes
20.1, pt. 13	0.039	-	1.014	2.984	0.983	-	-	-	5.02	Yes
20.1, pt. 17	0.048	-	1.024	2.975	0.981	-	-	-	5.03	Yes
20.1, pt. 18	0.026	-	1.021	2.979	0.993	-	-	-	5.02	Yes
20.1, pt. 22	-	-	1.008	2.983	1.008	-	0.020	-	5.02	Yes
35.1, pt. 39	0.034	-	1.012	2.985	0.934	-	0.010	0.019	4.99	Yes

Appendix Table AM

Sample	Accessory mineral(s)	Identification method	Certainty	Combined estimated abundance
1.1	Ap, Zrn	Optical (thin section)	Provisional (visual estimate)	~2-5% combined
8	Not recorded separately	-	-	Not recorded
11	Zrn and other minor phases	Optical (thin section)	Provisional (visual estimate)	~2-5% combined
13.1	Not separately quantified	-	-	Not recorded
14.2	Ttn, Fap, Zrn, Fl	SEM-EDS	Confirmed by EDS	Not recorded

16	Amp, Ep, Chl, Ap, Zrn	Optical (thin section)	Provisional (visual estimate)	~2-5% combined
20.1	Ap, Opq (Ap confirmed as Fap by EDS)	Optical (thin section) and SEM	Provisional (visual estimate)	~5-10% combined
28.1	Amp, Ep, Ilm, Fap, F-bearing Ttn, Fl, probable Cal	Optical (thin section) and SEM	Provisional (visual estimate)	~2-5% combined
35.1	Ilm, Mnz, Fap, Zrn, Ttn	Optical (thin section) and SEM	Provisional (visual estimate)	~2-5% combined
50	Ep, Ttn, Rt, Ilm, Mn-bearing Ilm confirmed by EDS; possible Ap and Fap identified visually only, not confirmed by a P-bearing EDS analysis	SEM-EDS (mixed certainty - see note)	EDS-confirmed except Ap, Fap (visual only)	Not quantified (no modal count; residual polished fragment, not a conventional thin section)

Note. Percentages assigned to additional or accessory minerals in the table above represent their estimated combined abundance, not the abundance of each listed mineral individually; individual proportions of phases such as zircon and monazite were not determined and are likely substantially lower than the combined estimate. Accessory minerals were excluded from the provisional main-phase modal estimates in Table and were too sparse for reliable individual visual estimates. Where estimated together with other minor phases, the combined additional, minor and accessory fraction was approximately 2-5 vol.%, increasing to approximately 5-10 vol.% in Sample 20. No separate estimate was made for Samples 8 or 13.1. For Sample 50, possible apatite and fluorapatite were both identified visually in SEM imagery but were not confirmed by a P-bearing EDS analysis. Abbreviations: Amp = amphibole; Ap = apatite; Bt = biotite; Chl = chlorite; Ep = epidote; Fap = fluorapatite; Fsp = feldspar; Grt = garnet; Ilm = ilmenite; Kfs = K-feldspar; Mc = microcline; Mnz = monazite; Ms = muscovite; Opq = opaque mineral; Pl = plagioclase; Px = pyroxene; Qz = quartz; Zrn = zircon. Cal = calcite; Fl = fluorite; Rt = rutile; Ttn = titanite.